NAIST-IS-DD0361022

Doctoral Dissertation

Structural basis for NHERF recognition by ERM proteins

Shin-ichi Terawaki

February 2, 2006

Department Bioinformatics and Genomics
Graduate School of Informatics Science
Nara Institute of Science and Technology

A Doctoral Dissertation
Submitted to the Graduate School of Information Science,
Nara Institute of Science and Technology
In partial fulfillment of the requirements for the degree of
Doctor of Science

Thesis Committee

Professor Toshio Hakoshima	(Supervisor)
Professor Naoki Ogasawara	(Co-supervisor)
Professor Chojiro Kojima	(Co-supervisor)

Structural basis for NHERF recognition by ERM proteins†

Shin-ichi Terawaki

Abstract

The Na^+/H^+ exchanger regulatory factor (NHERF) is a key adaptor protein involved in the anchoring of ion channels and receptors to the actin cytoskeleton through binding to ERM (ezrin/radixin/moesin) proteins. NHERF binds the FERM domain of ERM proteins, although NHERF has no signature Motif-1 sequence for FERM binding found in adhesion molecules. The crystal structures of the radixin FERM domain complexed with the NHERF-1 and NHERF-2 C-terminal peptides revealed a new peptide-binding site of the FERM domain specific for the 13-residue motif MDWxxxxx(L/I)Fxx(L/F) (Motif-2), which is distinct from Motif-1. This novel Motif-2 forms an amphipathic α-helix for hydrophobic docking to subdomain C of the FERM domain. We demonstrated competition between NHERF and adhesion molecule peptides for FERM binding. This suggested that the FERM domain might act as a molecular switch between Motif-1 and Motif-2 binding, thereby redirecting the ERM functions.

Key words

ERM proteins, FERM domain, NHERF, Cell adhesion, X-ray crystallography

---

† Doctoral Dissertation, Department of Bioinformatics and Genomics, Graduate School of Information, Nara Institute of Science and Technology, NASIT-IS-DD0361022, February 2, 2006

ERM 蛋白質による Na^+/H^+交換体制御因子認識の構造的基盤*

寺脇慎一

内容梗概

Na^+/H^+交換体制御因子(Na+/H+ Exchanger Regulatory Factor; NHERF)は、ERM (Ezrin/Radixin/Moesin) 蛋白質との相互作用を通して、イオンチャネルや受容体とアクチンフィラメントとの連結において鍵となるアダプター蛋白質である。NHERF は、ERM 蛋白質の FERM ドメインと結合するが､先に明らかにされている細胞接着分子の FERM ドメイン認識モチーフ (モチーフ 1) は存在しない。本研究では､radixin の FERM ドメインと NHERF-1 および-2 の C 末端領域との複合体の立体構造解析を通して、モチーフ 1 とは全く異なる MDWxxxxx(L/I)Fxx(L/F)という 13 残基の新規な FERM ドメイン結合モチーフ (モチーフ 2) を明らかにした。このモチーフ 2 は、両親媒性のαヘリックス構造を形成することで、FERM ドメインのサブドメイン C と主に疎水的な相互作用で結合する。さらに、モチーフ 2 の相互作用は、FERM ドメインの構造変化を引き起こすことで、モチーフ 1 の相互作用を阻害することを見出した。これらの結果は、FERM ドメインがモチーフ 1 とモチーフ 2 の間の分子スウィッチとして働くことで、ERM 蛋白質の機能を変換する可能性を示唆している。

キーワード
ERM 蛋白質、FERM ドメイン、NHERF、細胞接着、X 線結晶構造解析

---

*奈良先端科学技術大学院大学情報科学研究科情報生命科学専攻学位論文、NAIST-IS-DD0361022、2006 年 2 月 2 日

Content

List of Figures

1, Introduction

3, Results

List of tables

1, Introduction

3, Results

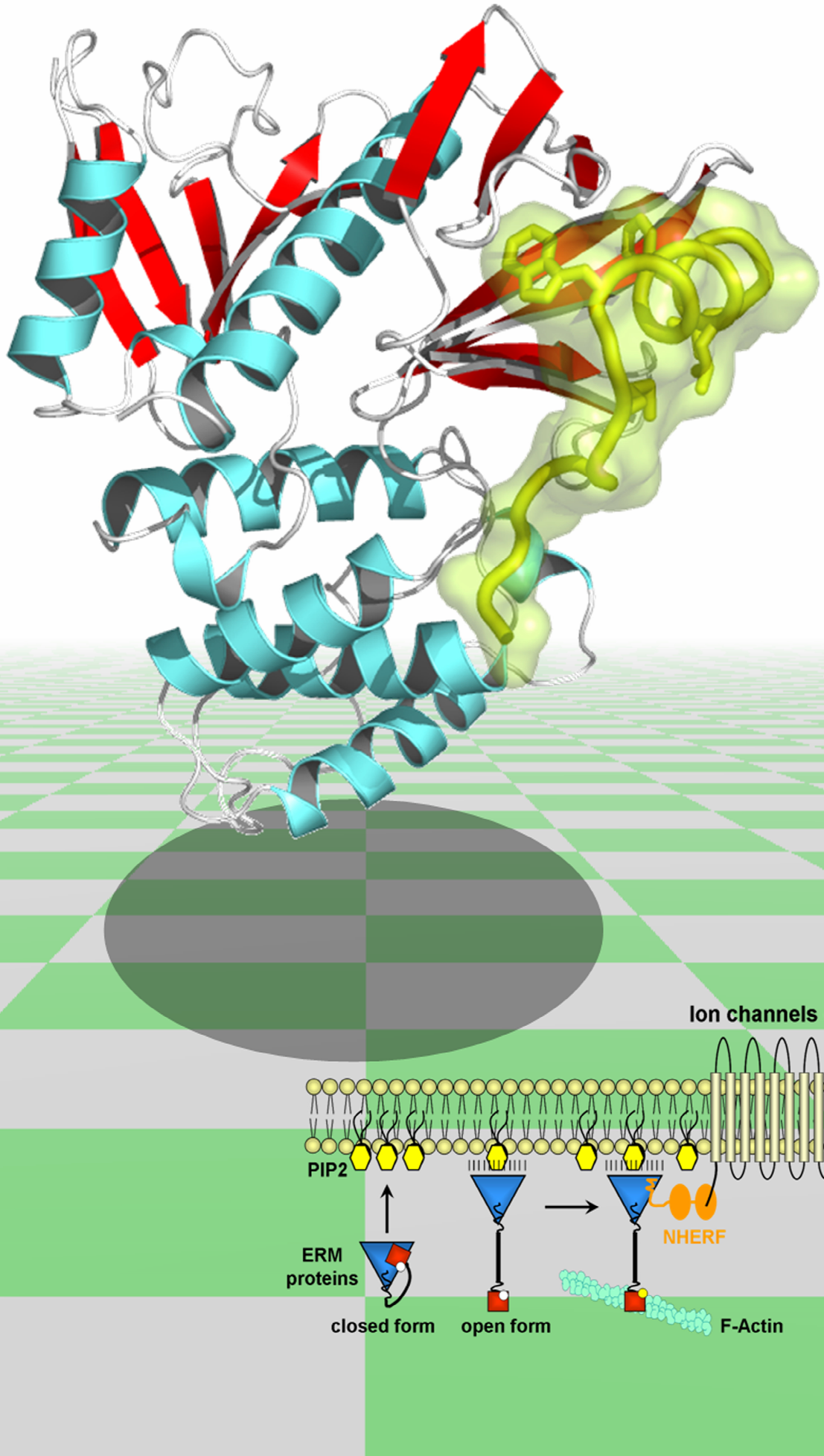
Ion channels or GPCRs
PIP2
NHERF
ERM
proteins
closed form
open form
F-Actin

1, Introduction

1.1 Ezrin-Radixin-Moesin (ERM) proteins

The cell polarity is a fundamental feature to establish functionally distinct apical and basolateral domains, or to define a front and back of a motile cell. Regulation of the cell polarity is achieved by interpreting signals that are derived from either within or outside the cell. Ultimately, this creates structurally and functionally distinct cortical domain structures that comprise the plasma membrane and cytoskeleton. The intracellular proteins to link between plasma membrane and cytoskeleton structure are necessary to formation and maintenance of these cortical domains (Albert B *et al.*, 2002).

Ezrin-Radixin-Moesin (ERM) proteins, which link actin filaments and plasma membranes, have been found in eukaryotic cells ranging from *Caenorhabditis elegans* to human (Bretscher *et al.*, 2002, Tsukita *et al.*, 1999). Three members of ERM proteins are closely related, having about 75% amino acid sequence identity (Bretscher A., 1983; Tsukita et al., 1989; Lankes et al., 1988 and 1991; Sato *et al.*, 1992) (Fig 1.1). Originally, ERM proteins are identified as components of structures at the cell surface, such as microbilli, membrane ruffles, cell adhesion sites and cleavage furrows where actin filament associated with plasma membrane. ERM proteins (about 580 amino acid residues) consist of three domains, an N-terminal globular domain, a central helical domain and a C-terminal domain (Fig 1.1). The N-terminal globular domain (~300 residues) is highly conserved (~80% identity) in ERM proteins and shows 32% identity to the equivalent domain in protein 4.1 (Fig 1.2). Thus, ERM proteins belong to the protein 4.1 superfamily which composed of proteins sharing a homology with this domain, called FERM (four point one ERM) domain (Chishti *et al.,* 1998). The FERM domain associates to the plasma membrane, while the C-tail domain binds to the filamentous (F)-actin

through their conserved actin-binding sites, which consist of 34 residues (550-583 for radixin) (Tsukita S *et al.*, 1994; Turunen *et al.*, 1994). These two domains are essential for linker protein between the plasma membrane and F-actin (Fig 1.3).

In cytosol, ERM proteins are negatively regulated by an intramolecular interaction between the FERM domain and the C-tail domain (Andréoli *et al.*, 1994; Gary *et al.*, 1995; Magendantz *et al.*, 1995). The crystallographic study of the moesin FERM domain complexed with the C-tail domain (the moesin FERM/C-tail domain complex) clarified the molecular basis of this intramolecular interaction (Pearson *et al.*, 2000). Activation of ERM proteins which requires separation of the two domains is regulates by phosphorylation and lipids, such as phosphatidylinositol. At least three kinases (Rho kinase, Protein kinase Cα (PKCα) and PKCθ) have been shown to phosphorylate the conserved threonine residue in the C-tail domain (Matsui *et al.*, 1998; Tran Quang *et al.*, 2000; Ng T, Parsons *et al.*, 2001; Pietromonaco *et al.*, 1998; Simons *et al.*, 1998). Phosphorylation of the threonine residue (Ezrin: 567, Radixin: 564, Moesin: 558) reduces the affinity of the C-tail domain for the FERM domain (Matsui *et al.*, 1998). Moreover, phosphorylated ERM proteins are found selectively in cell-surface structures (Oshiro et al., 1998; Hayashi et al., 1999). Regulation of the ERM proteins by binding to lipids is another pathway leading to the activation other than the C-tail domain phosphorylation. Biochemical studies have been shown that phosphatidylinositol (4, 5)-bisphosphate, PI(4, 5)P_2, binds the FERM domain of the ERM proteins and enhances target protein association with the full-length ERM proteins *in vitro* (Hirao et al., 1996; Yonemura et al., 1998; Yonemura et al., 2002) (Fig 1.3).

Both signaling events have been proposed to lie downstream the signaling pathway mediated by small GTPases of the Rho family, Rho, Rac, and Cdc42. These GTPases are

known to participate in the regulation of the actin cytoskeleton and various cell adhesions (Matsui *et al.*, 1999; Fukata *et al.*, 1998, Shaw *et al.*, 1998; Kotani *et al.*, 1997). ERM proteins have a role in the cellular cytoskeletal response to the Rho signaling pathway. Recent evidence has been shown that ERM proteins function upstream the Rho pathway through direct association with proteins that regulate Rho family. Rho guanine nucleotide dissociation inhibitor (RhoGDI), which is a negatively regulator, binds to the unmasked FERM domain of ERM proteins (Table 1.1). *In vitro* studies indicate that the FERM domain stimulates release of inactive Rho GTPase from RhoGDI, and thereby Rho GTPase is activated by exchange of GDP for GTP (Takahashi *et al.*, 1997). ERM proteins also interact with Rho specific guanine nucleotide exchange factor Dbl, although this interaction does not affect the exchange reaction (Takahashi *et al.*, 1998; Vanni *et al.*, 2004; Lee *et al.*, 2004). These finding implies a feedback loop for the Rho signaling pathway.

1.2 Membrane targets of the ERM proteins

Membrane targeting of ERM proteins by the N-terminal FERM domain is the most important function to regulate specific cortical domain. PI(4,5)P_2 is one of the FERM domain interacting molecules and regulates not only activation but also localization of the ERM proteins in plasma membrane (Hirao *et al.*, 1996). Crystallographic studies of the radixin FERM domain and its complex with inositol-1, 4, 5-triphosphate (Ins(1,4,5)P_3) that is head group of the PI(4,5)P_2 have provided insight into the conformation of the FERM domain and the PI(4,5)P_2 recognition (Hamada *et al.*, 2000) (Table 1.2). The FERM domain was found to consist of three subdomains: subdomains A (residues 1-83), B (96-195) and C (204-297). Subdomain A has an ubiquitin fold and subdomain B has a helix bundle fold

similar to an acyl-CoA binding protein. Subdomain C shows structural homology to an adaptable module that is described as phosphotyrosine binding (PTB) and pleckstrin homology (PH) domains. In the Ins(1,4,5)P_3-bound form structure, Ins(1,4,5)P_3 has been shown to bind in the basic groove between subdomain A and subdomain C.

For the major target proteins of the FERM domain, two types of interactions with membrane proteins have been documented: a direct association of the FERM domain with the cytoplasmic tail of transmembrane proteins and an indirect association with the tail of membrane proteins through scaffolding proteins (Table 1.1). Transmembrane proteins which directly associate with the FERM domain of ERM proteins play a key role in cell adhesion and cell-cell communication. These transmembrane proteins include CD44, CD43, and intercellular adhesion molecule (ICAM) -1, -2 and -3 (Tsukita *et al.*, 1994; Yonemura *et al.*, 1998; Legg *et al.*, 1998; Heiska *et al.*, 1998). CD44 is a cell surface hyaluronate receptor precisely co-localized with ERM proteins in cultured fibroblasts. CD43 is a cell surface glycoprotein of the sialomutin family and ICAM-1, -2, -3 is the immunoglobulin superfamily member proteins. A crystallographic study of the radixin FERM domain bound to the ICAM-2 cytoplasmic tail has been reported (Hamada *et al.*, 2003). This complex structure revealed that the FERM domain recognizes the signature sequence RxxTYxVxxA (motif-1).

1.3 Cytoplasmic targets of ERM proteins

In addition to direct association with cytoplasmic tails of adhesion molecules, ERM proteins interacts with Na+/H+ exchanger regulatory factors (NHERF), which is the best-studied adaptor protein that is highly expressed in epithelial cells and localized at the apical plasma membrane (Reczek *et al.*, 1997; Yun *et al.*, 1998) (Table 1.2). Two NHERF

isoforms (NHERF-1 and NHERF-2) show 55% sequence identity and have also been referred to as ERM-binding phosphoprotein 50 (EBP50) and Na^+/H^+ exchanger 3 kinase A regulatory factor (E3KARP), respectively. Human NHERF-1 is a 358-residue protein containing two PSD-95/Dlg/ZO-1 homology (PDZ) domains (PDZ1: 13-93 and PDZ2: 153-233) followed by ~120 C-terminal residues that contain about 30 residues (331-358 residues) of the FERM domain binding region (Weinman *et al.*, 2000; Voltz *et al.*, 2001) (Fig 1.4). PDZ domains typically recognize a specific consensus sequence in the extreme C-terminus of their target proteins. The growing list of potential NHERF targets includes nine ion channels/transporters such as Na^+/H^+ exchanger 3 (NHE3) (Weinman *et al.*, 1995) and the cystic fibrosis transmembrane conductance regulator (CFTR) (Wang *et al.*, 1998), seven G-Protein-Coupled Receptors (GPCRs) containing the β_2 adrenergic receptor (β_2AR) (Hall *et al.*, 1998) and the Parathyroid Hormone 1 Receptor (PTH1R) (Mahon *et al.*, 2002), in addition to cytoplasmic signaling, scaffold and nuclear proteins. Platelet-Derived Growth Factor Receptor (PDGFR) (Maudsley *et al.*, 2000) and Epithelial Derived Growth Factor Receptor (EGFR) (Lazar *et al.*, 2004) are also NHERF targets. Molecular and cellular studies over the past decade have demonstrated that NHERF is a key regulator for targeting of these membrane proteins, and for controlling their activity (Table 1.3).

NHERF-1 and NHERF-2 are essential mediators of hormonal signals that inhibited NHE3 activity in renal (Weinman *et al.*, 1993) and gastrointestinal epithelial cells (Lamprecht *et al.*, 1998). This complex is necessary for anchoring to the F-actin and membrane recruitment of the Protein kinase A (PKA), which binds to the ezrin and promotes phosphorylation of the NHE3 cytoplasmic domain (Dransfield *et al.*, 1997; Kurashima *et al.*, 1999; Weinman *et al.*, 2000). Cytoskeleton anchoring and phosphorylation induced endocytic internalization of NHE3 from plasma membrane (Hu

et al., 2001). NHERF also have been shown to participate in regulation of Na/Pi cotransporter and Na-K-ATPase through interaction with NHERFs (Mahon *et al.*, 2003; Khundmiri *et al.*, 2005). However, CFTR, which is an ATP-binding cassette transporter, has been shown that NHERF binding is enhanced to the Cl^- ion transport activity (Sun *et al.*, 2000; Raghuram *et al.*, 2001). In additional to associating with ion channels, NHERF also bind to the C-terminal of agonist-occupied β_2AR via their N-terminal PDZ1 domain (Hall *et al.*, 1998). These studies revealed a long standing paradox whereby some cAMP elevating hormones inhibited NHE3 while others, like β_2AR agonists, increased NHE3 activity.

PDGFR, which is the receptor tyrosine kinase, associates with the PDZ1 domain of NHERF-1 and NHERF-2 (Maudsley *et al.*, 2000). PDGFR, like other receptor tyrosine kinase, is activated through ligand-induced dimerization and transphosphorylation of the clustered receptors, and NHERF promotes PDGFR dimerization in part due to NHERF's own ability to form dimmers (Fouassier *et al.*, 2000; Shenolikar *et al.*, 2001). In this manner, NHERF enhances growth factor signaling and actives mitogenic signals by MAPK.

1.4 Aim of this study

The FERM domain of the ERM proteins binds adhesion molecules or NHERFs, while the FERM domain binding regions of these target proteins have little amino acid sequence identity, although these regions are defined to short peptide regions consisting of less than 30 residues (Yonemura *et al.*, 1998; Reczek *et al.*, 1997; Yun *et al.*, 1998). In order to clarify how the FERM domain recognizes NHERF, I determined the crystal structures of the radixin FERM domain complexed with the NHERF-1 and NHERF-2 peptides. The

complex structures revealed a new peptide-binding site on the FERM domain and a novel signature sequence MDWxxxxx(L/I)Fxx(L/F) (motif-2) of NHERF for the FERM-binding. The NHERF-binding motif forms an amphipathic α helix for hydrophobic docking to the groove formed by two β sheets from the β-sandwich of subdomain C. This binding site is distinct from the ICAM-2 binding site at the groove formed by strand β5C and helix α1C (Hamada *et al.*, 2003) (motif-1). Thus, the FERM domain provides two distinct binding sites for two classes of target proteins with different specificity. We also provide *in vitro* evidence for the interference concerning the binding of NHERF and adhesion molecules such as ICAM-2 to the FERM domain, suggesting a redirection of ERM function.

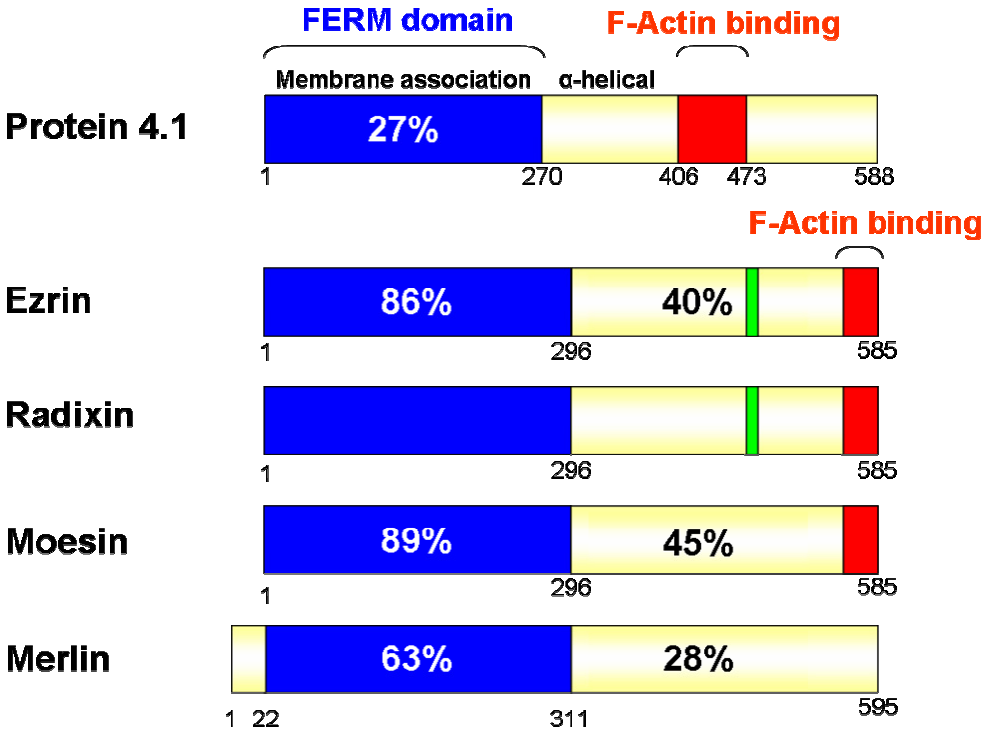

Figure 1.1 Protein 4.1, the ERM (Ezrin/Radixin/Moesin) proteins and Merlin.

These proteins contain a FERM domain at the N-terminal region. Sequence identity to radixin is shown. Protein 4.1 shows poor sequence identity with the ERM proteins and Merlin. ERM proteins have a C-terminal actin binding region, whereas Merlin does not. Ezrin and radixin have a Proline rich region (green), function of which is unknown.

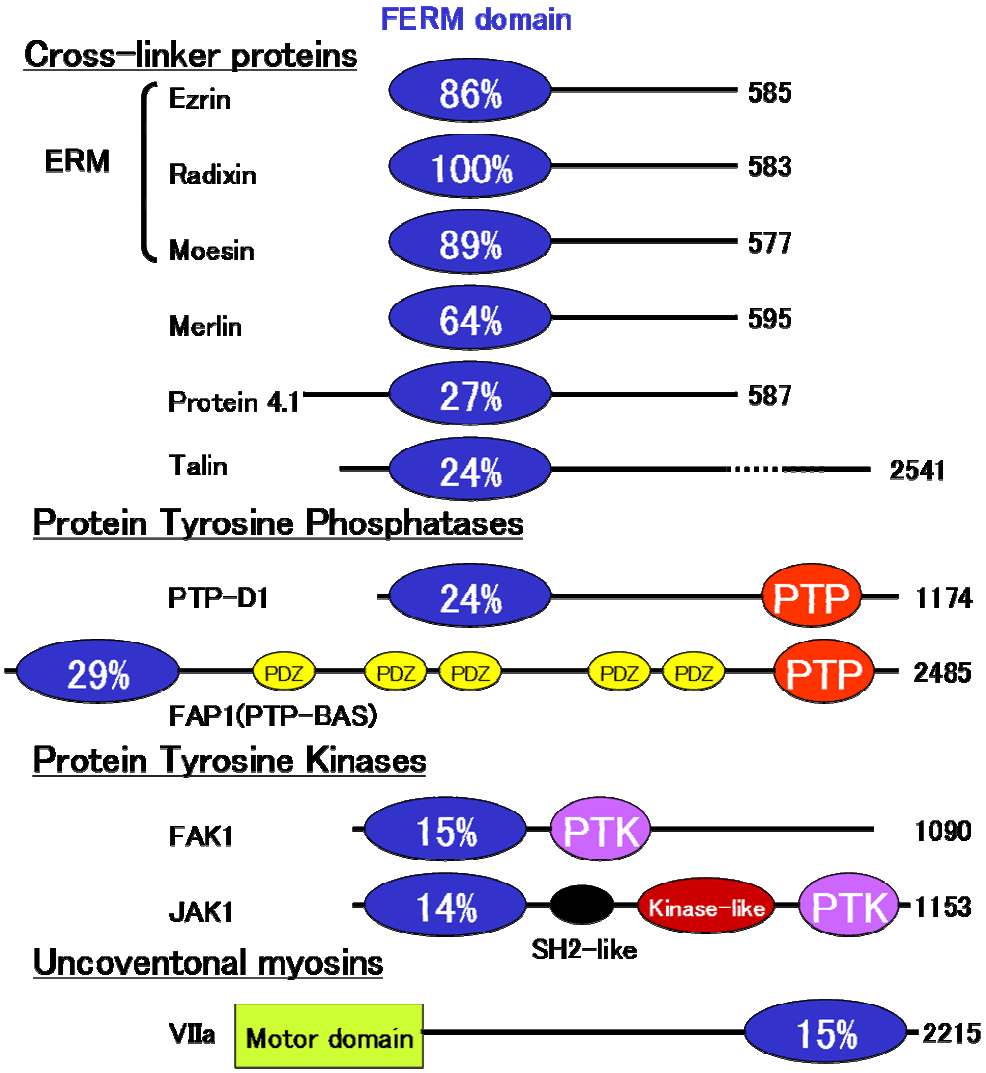

Figure 1.2 Protein 4.1 superfamily

Proteins that contain FERM domain belong to the Protein 4.1 superfamily. This family is comprised of numerous membrane associated signaling and cytoskeletal proteins. Additional domains include the structurally related to the Src homology-2 (SH2-like), protein tyrosine kinase (PTK), PSD95/Dlg/ZO-1 homology (PDZ), proteins tyrosine phosphatase (PTP) and the myosine subfragment-1 (S-1; a motor domain) domains. Sequence identity to radixin is shown.

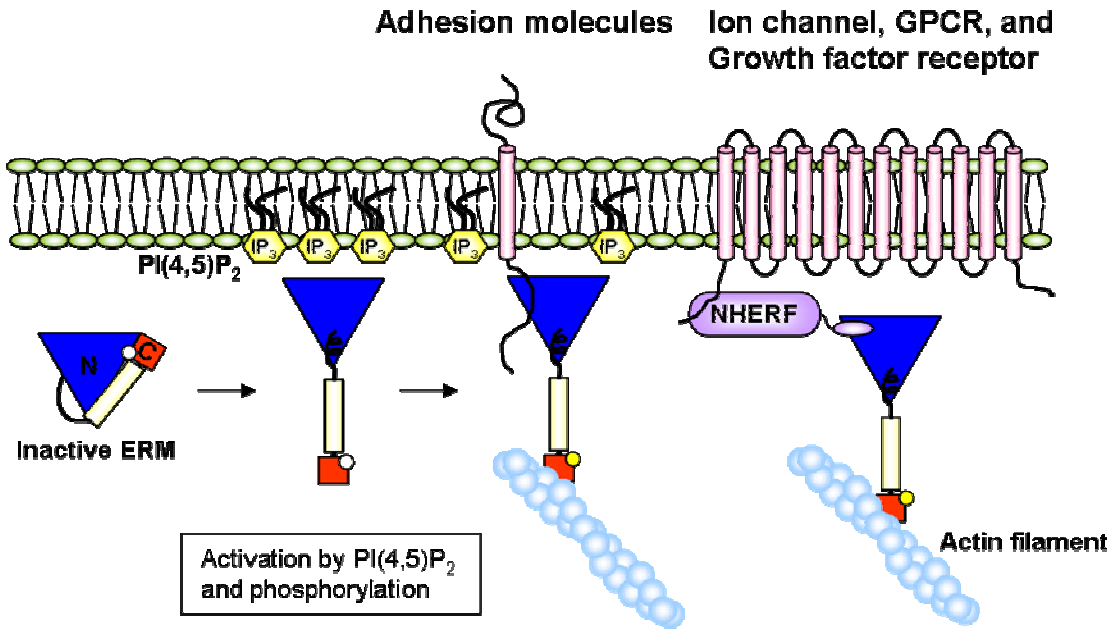

Figure 1.3 Membrane targeting of ERM proteins

ERM proteins are negatively regulated by an intramolecular interaction between the FERM domain and the C-tail domain in cytosol. The production of PI(4,5)P2 by Rho GTPase signaling recruits ERM proteins to the plasma membrane, which place them in a location to phosphorylate the C-terminal conserved threonine. These processes induce the dissociation of the C-tail domain from the FERM domain. Activated ERM proteins can participate in formation of an actin filament-plasma membrane linkage by direct association with adhesion molecules such as CD44, CD43, ICAM-1, -2, -3, or indirect through scaffolding proteins, NHERF.

Table 1.1 Proteins that bind the FERM domain of ERM proteins

Adhesion molecules
CD44, ICAM-1, ICAM-2, ICAM-3, L-selectin (Ivetic *et al.*, 2001)
Ion transporter
NHE1 (Denker *et al.*, 2000)
Signaling molecules
RhoGDI, Dbl, FAK (Poullet *et al.*, 2001), PI3K (Gautreau *et al.*, 1999), Hamartin (Lamb *et al.*, 2000), N-WASP (Manchanda *et al.*, 2005)
Others
CD43, CD95 (Parlato *et al.*, 2000), PSGL-1(Alonso-Lebrero *et al.*, 2000), NEP (Iwase *et al.*, 2004)
Scaffolding proteins
NHERF1/EBP50, NHERF-2/E3KARP, SAP97 (Bonilha *et al.*,2001)
Syndecan-2 (Granes *et al.*, 2000)

ICAM: Intercellular Adhesion Molecule, RhoGDI: Rho GDP Dissociation Inhibitor, Dbl: Diffuse B cell Lymphoma, FAK: Focal Adhesion Kinase, PI3K: Phosphatidylinositol-3 kinse, HRS: Hepatocyte growth factor receptor Regulated Substrate, N-WASP: Neuronal-Wiskkot Aldrich Syndrome Protein, PSGL-1: P-Selectin Glycoprotein-1, NEP: Neutral Endpeptidase 2.4.11, SAP97: Synapse-Associated Protein 97

Table 1.2 Structural studies of the FERM domain

Molecule	Partner	PDB ID	Reference
Protein 4.1	non	1GG3	Han *et al.*, 2000
Ezrin	non	1NI2	Smith et al., 2003
Moesin	non	1E5W	Edwards *et al.*, 2001
Moesin	C-tail domain	1EF1	Pearson *et al.*, 2000
Radixin	non	1GC7	Hamada *et al.*, 2000
Radixin	Ins (1, 4, 5) P_3	1GC6	Hamada *et al.*, 2000
Radixin	ICAM-2	1J19	Hamada *et al.*, 2003
Merlin	non	1ISN	Shimizu *et al.*, 2002
		1H4R	Kang *et al.*, 2002
Talin	non	1MIX	Garcia-Alvarez *et al.*, 2003
Talin	Integrin	1MK7	Garcia-Alvarez *et al.*, 2003
		1MK9	Garcia-Alvarez *et al.*, 2003
Talin	PtdIns Kinase I-γ	1Y19	de Pereda *et al.*, 2005
FAK	non	2AEH	Ceccarelli *et al.*, 2005
		2AL6	Ceccarelli *et al.*, 2005

FAK: Focal Adhesion Kinase

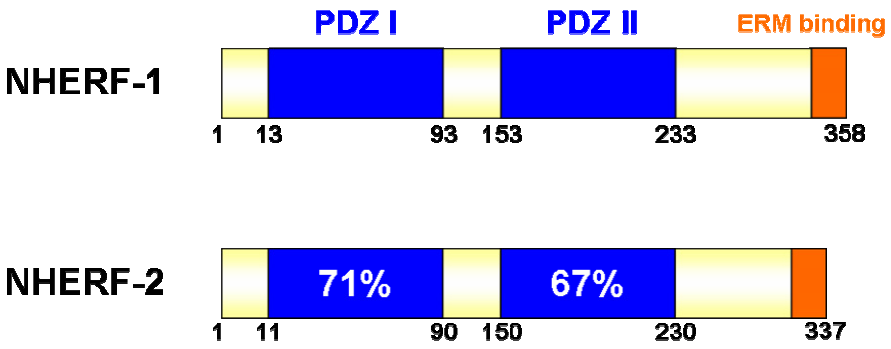

Figure 1.4 Domains of NHERF

NHERF contains two tandem PDZ domains. These PDZ domains bind to the conserved sequence of the membrane proteins (NHERF binding partner shows in Table 1.3). C-terminal regions of about 30 amino-acid residues bind the FERM domain of ERM proteins.

Table 1.3 Proteins that bind the PDZ domains of the NHERF

PDZI interacting proteins
Ion transporters: CFTR, H+-ATPase, NPT2
Signaling receptors: β2-Adrenergic receptor, P2Y1R, PDGFR
Signaling proteins: PLCβ1, GRK6A
PDZII interacting proteins
Ion transporters: NHE3
Signaling receptors: PTHR
Signaling proteins: YAP65

CFTR: Cystic Fibrosis Transmembrane Conductance Regulator, NPT2: Na/Pi Cotransporter Type 2A, P2Y1R: Purinergic 2 Y 1 Receptor, PDGFR: Platelet Derived Growth Factor Receptor, PLCβ1: Phospholipase Cβ1, GRK6A: G-protein Coupled Receptor Kinase 6A, NHE3: Na^+/H^+ Exchanger, PTHR: Parathyroid Hormone Receptor, YAP65: Yes-Associated Protein 65

2, Materials and methods

2.1 Protein expression and sample preparation for the protein crystallization

The FERM domain (residues 1-310) of mouse radixin was expressed in BL21 (DE3) RIL cells containing plasmid pGEX4T-3 as a fusion protein with glutathione S transferase (GST) (Matsui *et al.*, 1998). Details of the purification scheme of this domain have been described previously (Hamada *et al.*, 2000). In addition to the scheme, heparin Sepharose column chromatography was applied at the final step. Heparin Sepharose, which was reported to bind to the moesin FERM domain (Lankes *et al.*, 1988), has ionic groups similar to Ins(1,4,5)P_3. The purified samples were verified with matrix-assisted laser desorption / ionization time-flight mass spectroscopy (MALDI-TOF MS; PerSeptive Inc.) and N-terminal analysis (M492, Applied Biosystems), and then was concentrated to 50 mg/ml for crystallization.

The peptides corresponding to the C-terminal regions of human NHERF-1 and NHERF-2 were purchased from Sawady Technology (Tokyo Japan). For crystallization, these peptides were dissolved to 5.3 mM concentration in a buffer containing 70 mM NaCl and 10 mM MES-Na pH 6.8, 1mM DTT. These peptides sequence show at Table 3.6.

2.2 Analysis of the protein-peptide interaction

Binding assay of NHERF peptides to the FERM domain was performed by surface plasmon resonance measurements using a Biacore Biosensor instrument (BIAcore 3000, Pharmacia Biosensor). Each biotinylated peptide was immobilized on the surface of a SA (Strept Avidin) sensor chip. The purified FERM domain was injected on the peptide surfaces. All binding experiments were performed at 25 degree with a flow rate of 30 μl/ml in HBS-EP buffer (10 mM HEPES-Na pH 7.4, 150 mM NaCl, 1 mM EDTA, 0.05%

surfactant P20). The kinetic parameters were evaluated using the BIA evaluation software (Pharmacia). The binding affinity for several mutated (replacement with alanine) or truncated NHERF-1 peptides also were examined using equilibrium SPR measurements in a similar manner to that of wild type NHERF-1 peptide binding assay.

2.3 Protein crystallization

The radixin FERM domain and the NHERF-1 peptide were mixed in a 1:1 molar ratio (each 0.33 mM) in a solution of 185 mM NaCl, 10 mM MES-Na pH 6.8 and 1 mM DTT. Crystallization conditions were searched using the hanging-drop vapor-diffusion method at 277 K. Crystals of the complex were obtained in 3 days by combining 1 μl of protein solution with 1 μlof reservoir solution containing 10% polyethylene glycol 4000 (PEG 4K), 5% 2-propanol, 100 mM HEPES-Na pH 7.5. The crystals grew up to maximal dimensions of 0.2×0.5×0.1 mm. The obtained crystals were resolved in an aliquot of water for MALDI-TOF MS to verify that the crystals contain both the radixin FERM domain and the NHERF-1 peptide. We observed a peak of 3400.4 Da corresponding to the calculated value of 3400.9 Da for the NHERF-1 peptide, as well as a peak corresponding to the radixin FERM domain.

Crystals of the complex between the radixin FERM domain and the NHERF-2 peptide were obtained under a condition similar to that of the FERM/NHERF-1 complex. The radixin FERM domain and the NHERF-2 peptide were mixed in a 1:1 molar ratio (each 0.45 mM) in the same solution as that for the FERM/NHERF-1 complex. Crystals of the complex were obtained in 2 weeks by combining 1.3 μl of protein solution with 0.7 μlof the same reservoir solution as that for the FERM/NHERF-1 complex. The crystals grew up to maximal dimensions of 0.2×0.4×0.01 mm. It was also confirmed by MALDI-TOF MS

that the crystals contain both the radixin FERM domain and the NHERF-2 peptide. We observed a peak of 3507.82 Da corresponding to the calculated value of 3508.09 Da for the NHERF-2 peptide, as well as a peak corresponding to the radixin FERM domain.

2.4 X-ray data collection

For X-ray diffraction experiments, crystals were transferred stepwise into a cryoprotective solution containing 20% PEG 200, 20% PEG 4K, 10% 2-propanol and 100 mM HEPES-Na pH 7.5 for flash-cooling. X-ray diffraction data of the FERM/NHERF-1 complex were collected with an ADSC Quantum 4R detector installed on the BL40B2 beamline at SPring-8 using flash-frozen crystals. The data collection was performed with a total oscillation range of 180° with a step size of 0.5° for an exposure time of 60 sec. The camera distance was 180 mm. Crystals were found to diffract to a resolution of 2.5 Å and to belong to space group $P2_12_12_1$ with unit-cell parameters, a=69.38 (2), b=146.27 (4), c=177.76 (7) Å. All data were processed with the programs *MOSFLM* (Leslie, 1992) and *SCALA* (Collaborative Computational Project, Number 4, 1994). The total number of observed reflections was 459,178, which gave 62,668 unique reflections. The resulting data gave an R_{sym} of 6.5% (34.9% for the outer shell, 2.64–2.50 Å) with a completeness of 99.2% (98.9% for the outer shell). The estimated mosicity of the crystal was 0.30°. Assuming the presence of four complexes in the asymmetric unit, the calculated value of the crystal volume per protein mass (V_M; Matthews, 1968) is 2.81 $Å^3\,Da^{-1}$. This value corresponds to a solvent content of approximately 56%.

X-ray diffraction data of the FERM/NHERF-2 complex were collected with a MAR CCD detector installed on the BL41XU beamline at SPring-8 using flash-frozen crystals, with a total oscillation range of 82.5° with a step size of 0.5° for an exposure time of 5 sec.

Crystals were found to belong to space group $P2_12_12_1$ with unit-cell parameters, a=68.63 (2), b=144.37 (4), c=177.94 (7) Å, which were nearly isomorphous to the crystals of the FERM/NHERF-1 complex. Intensity data at 2.8 Å were processed using DENZO/SCALEPACK (Otwinowski *et al.*, 1997). The total number of observed reflections was 118,872, which gave 41,789 unique reflections with an R_{sym} of 8.5% (31.7% for the outer shell, 2.90-2.80 Å) and a completeness of 95.0% (95.0% for the outer shell).

2.5 Structural determination and refinement

Initial phases were calculated by molecular replacement using a search model based on the free form structure of the radixin FERM domain (Hamada *et al.*, 2000) with the program *AMoRe* (Navaza., 1994). The solutions were estimated by *R*-factor (*R*) and Correlation coefficient (*C*). *R* is calculated by equation 2.1 that is the sum of the absolute difference between observed $|F_{obs}|$ and calculated $|F_{cal}|$ over sum of $|F_{obs}|$. *C* is expressed by equation 2.2. The advance of this value over the *R* is that it is scale insensitive.

$$R = \frac{\sum_{hkl}(|F_{obs}| - \kappa|F_{calc}|)}{\sum_{hkl}|F_{obs}|} \qquad \text{----------(2.1)}$$

$$C = \frac{\sum_{hkl}(|F_{obs}|^2 - \overline{|F_{obs}|^2}) \times (|F_{calc}|^2 - \overline{|F_{calc}|^2})}{[\sum_{hkl}(|F_{obs}|^2 - \overline{|F_{obs}|^2})^2 \sum_{hkl}(|F_{calc}|^2 - \overline{|F_{calc}|^2})]^{\frac{1}{2}}} \qquad \text{----------(2.2)}$$

The Solution that has low value of the R and high value of the *C* is selected for the most agreeable solution (Table 3.2).

Following rigid-body refinement of the search model performed with the program

CNS (Brünger *et al.*, 1998), the phases were improved by solvent flattening and histogram matching using Solomon (Abrahams *et al.*, 1996). An initial model of the peptide was built into the electron density map using the graphics program *O* (Jones *et al.*, 1991) and refined by the methods of simulated annealing in *CNS* (Brünger *et al.*, 1998) and restraint least-squares refinement in *REFMAC* (Murshudov *et al.*, 1997). In the peptide models, the side chains of residues 339-342, 350 and 353 were poorly defined in the current map and the structure with replaced alanines. The structure of the FERM-NHERF-2 complex was solved by molecular replacement with the FERM/NHERF-1 structure and refined as shown in Table 3.3.

2.6 Structure Inspection

The stereochemical quality of the model was monitored using the program PROCHECK (Laskowski et al., 1993). There are two outliers in the Ramachandran plot, Asp252 in the type II reverse turn between strands ß5C and ß6C, and Lys262 in loop ß6C-ß7C (Fig.3.2). Ribbon representations of the main-chain folding of the molecule were drawn using the program Molscript (Kraulis, 1991) and Pymol (http://pymol.sourceforge.net/), while molecular surface representations were drawn using the program GRASP (Nicholls et al., 1991). A schematic diagram of the interactions was prepared with the program LIGPLOT (Wallace et al., 1995).

2.7 Structural comparison of the FERM domain

Structural studies of the FERM domain of other proteins and complexes with adhesion molecule such as ICAM-2 or membrane component, Ins(1,4,5)P_3 were reported (Table 1.2). Comparison of our complex structure with these structures exhibits how the

interaction with NHERF induces to structural change. Superposition of the FERM domains carried out *LSQKAB* (Collaborative Computational Project, Number 4, 1994).

2.8 Interference experiments

Interference between NHERF and adhesion molecules binding to the FERM domain was tested by SPR analysis of the binding of purified radixin FERM domain to the cytoplasmic tail peptides of ICAM-2 (28 residues), ICAM-1 (28), VCAM-1 (20) and CD44 (37) immobilized on the sensor chips. The purified radixin FERM domain (100 nM) was injected into the sensor chips. Similarly, effects of $PI(4,5)P_2$ on FERM binding to the NHERF or ICAM-2 peptide were examined by SPR analysis of the binding of radixin FERM domain to the peptides. The purified radixin FERM domain (100 nM) was injected into the sensor chips with or without soluble di-butanoyl-$PI(4,5)P_2$. We measured the binding of the FERM domain to $PI(4,5)P_2$-containing lipid vesicles immobilized to the L1 sensor chips by SPR measurements to estimate the K_d value. The vesicles were prepared with $PI(4,5)P_2$-containig POPC (1-palmitoyl-2-oleoyl-sn-glycero-3-phosphocholine) by rehydration of dried lipids in 5 mM Na_2HPO_4, 5 mM KH_2PO_4 (pH 7.4), and 150 mM NaCl. All samples were injected into both the peptide-linked and non-linked sensor chips for correction of background signals.

3, Results

3.1 Structural determination and overall structure of the radixin-NHERF complex

Crystals of the radixin FERM domain bound to each NHERF peptide were obtained using NHERF-1 and -2 peptides consisting of the 28 C-terminal residues (^{331}KERAHQKRSS KRAPQMDWSK KNELFSNL^{358} and ^{310}KEKARAMRVN KRAPQMDWNR KREIFSNF^{337}), respectively (Terawaki *et al.*, 2003) (Fig. 3.1). Our binding assay showed that the peptides bind the FERM domain with high affinity and dissociation constant K_d in the nanomolar range (described below). The structure was determined by molecular replacement using the free radixin FERM domain (Hamada *et al.*, 2000) (Table. 3.2). The FERM-NHERF-1 and FERM-NHERF-2 complexes were refined to 2.5-Å and 2.8-Å resolution, respectively (Table 3.3). Crystals of the radixin FERM domain bound to NHERF-1 or -2 peptides contained four molecular complexes per asymmetric unit (Fig. 3.2). The structure of four crystallographic-independent complexes was essentially the same in both crystals. Moreover, no significant overall structural deviation was found in the FERM domains of the two complexes with averaged root-mean-square (r.m.s.) deviations in C_α-carbon atoms being 0.35 Å (Table. 3.4). Our discussion will therefore focus on the structure of the FERM/NHERF-1 complex followed by reference to a local structural change in the NHERF-2 peptide.

The current structure of the FERM-NHERF-1 complex includes 1186 residues of the FERM domain, 80 residues of the NHERF-1 peptide and 617 water molecules. The FERM-NHERF-2 complex includes 1176 residues of the FERM domain, 70 residues of the NHERF-2 peptide and 163 water molecules (Table. 3.3). No model of the NHERF-1 peptide was built for the N-terminal 8 residues. The side chain of the residues 339-342, 350 and 353 were poorly defined in the current map and the structure with replaced alanines. The

NHERF-2 peptides have no models for the N-terminal 10 or 11 residues. As previously reported (Hamada *et al.*, 2000; Hamada *et al.*, 2003), the FERM domain consists of three subdomains A, B and C. Subdomain C, which folds into a standard seven-stranded β-sandwich (strands β1C-β7C) with one long capping α-helix (α1C). Subdomain A has a typical ubiquitin fold while subdomain B has an α-helix bundle structure. The NHERF-1 and NHERF-2 peptides are located at the molecular surface of subdomains C and B (Fig. 3.4a). All the peptide binding sites faced toward the large solvent channels in the crystal and three complexes have no crystal contact involving the peptide residues. The other complex has a few crystal contacts involving the peptide residues (Asn357 and Leu358), while no changes were found in the peptide conformation compared with the peptides having no crystal contacts. Therefore, I think that the crystal contacts do not affect the peptide conformation and the binding mode to the FERM domain.

3.2 Structure of the FERM domain in the NHERF bound form

Compared with the free form, Ins(1,4,5)P_3 bound (Hamada *et al.*, 2000) and ICAM-2 bound forms (Hamada *et al.*, 2003), the overall r.m.s deviations of the NHERF-1 bound FERM domain are relatively large (free: 0.95 Å, Ins(1,4,5)P_3 bound: 0.95 Å, ICAM-2 bound: 1.48 Å) and, especially, the ICAM-2 bound form shows the largest deviation (Fig. 3.4b). The pair-wise superposition of each subdomain showed that the major deviation is associated with subdomain C (more than 1.0 Å) that binds the NHERF peptide, while the deviations pertaining to subdomain A and B are relatively small. The r.m.s. deviations obtained from the pair-wise superposition of overall and each subdomain are shown in Table 3.5.

3.3 NHERF peptide conformation

The NHERF peptides consist of two regions (Fig. 3.5a). The N-terminal region (residues 331-345 for NHERF-1) includes basic residues, while the C-terminal region (346-358) contains nonpolar residues. The structured regions of the NHERF-1 peptide (blue in Fig. 3.4a) form a N-terminal loop (residues 339-347) followed by a 3-turn amphipathic α helix consisting of the extreme C-terminal 11 residues (348-358). At the helix surfaces, two aromatic side chains from Trp348 and Phe355 protrude from one side (Fig. 3.5b). The aliphatic part of the Lys351 side chain makes contact with the aromatic ring of Trp348. On another side of the helix, three aliphatic side chains (from Met346, Leu354 and Leu358) interact side by side. These aromatic and aliphatic residues form hydrophobic molecular surfaces on the helix. The other side of the helix is occupied by polar residues including poorly-defined Lys350 and Glu353, which protrude toward the solvent region. The helix is stabilized by the side chain of Asp347, which forms the N-terminal cap of the α helix by hydrogen bonding to the main-chain amide group(s) of Ser349 and/or Lys350 (Fig. 3.5d). The helices of the NHERF-1 peptides in four crystallographic-independent complexes are well overlaid with a small averaged r.m.s. deviation (0.29 Å). In contrast to the rigidity of the helices, most of residues in the N-terminal loop region seem to be flexible in our complexes. In fact, the structure of the N-terminal loop regions of the four independent NHERF peptides displayed different conformations (Fig. 3.6, *left*).

3.4 NHERF peptide recognition

The interface between the NHERF-1 peptide and the FERM domain buries 1,630 $Å^2$ of the total accessible surface area including both the peptide and the domain. The

C-terminal helix of the peptide docks to the groove between two β sheets, the four-stranded sheet β1C-β2C-β3C-β4C (sheet β1C-β4C) and the three-stranded sheet β5C-β6C-β7C (sheet β5C-β7C), from the β-sandwich of subdomain C (Fig. 3.7a). The contacts are predominantly mediated by nonpolar interactions involving side chains (Fig. 3.7b, c). The groove provides two hydrophobic pockets for accommodation of Trp348 and Phe355 from the NHERF-1 peptide (Fig. 3.5, *right*). These two residues are completely buried at the interface. The two pockets are separated by two residues, Phe240 from sheet β1C-β4C and Phe267 from sheet β5C-β7C. The pocket for Trp348 is formed by strands β4C (Phe240), β6C (Ile257 and Pro259) and loop β6C-β7C (Pro265). The pocket for Phe355 is formed by strands β7C (Phe267 and Phe269), β2C (Leu216) and the aliphatic part of the Lys211 side chain from loop β1C-β2C. Thus, both pockets are formed by residues from both β1C-β4C and β5C-β7C sheets (Fig. 3.8). In addition to the aromatic residues, Met346, Leu354 and Leu358 from the NHERF-1 peptide align their side chains together toward the hydrophobic groove of subdomain C and associate with nonpolar residues (Ile238, Ile227 and Leu216) from sheet β1C-β4C.

In contrast to the wealth of nonpolar intermolecular interactions, only six hydrogen bonds were found between the NHERF-1 peptide and subdomain C. These interactions involve side chains from three NHERF-1 residues (Trp348, Lys351 and Asn352) and from three radixin residues (Asn210, Thr214 and Glu244), as well as main chains (Fig. 3.7b, c). The terminal carboxylate group of the C-terminal end residue (Leu358 of NHERF-1) forms bifurcated hydrogen bonds with the side chains of Asn210 and Thr214 from the FERM domain. The side chain of Asn210 also forms a hydrogen bond with the main chain of NHERF-1 Phe355. The N-terminal loop of the NHERF-1 peptide protrudes toward the molecular surface between subdomains B and C (Fig. 3.4a). Interestingly, this molecular

surface contains many acidic residues (Fig. 3.6), suggesting the presence of electrostatic interactions between the positively-charged N-terminal basic residues of the peptide and negatively-charged residues located at the acidic groove formed by subdomains B and C.

In the FERM-NHERF-2 complex, the peptide-protein interactions are similar to those described above, while Ile333 and Phe337 of NHERF-2 replace Leu354 and Leu358 of NHERF-1. These replacements induce local conformational changes in the C-terminal part of the NHERF-1 helix (Fig. 3.5e), resulting in modified side-chain packing of two residues against the groove of subdomain C. This double replacement would enable a closest side-chain packing of Phe/Ile in NHERF-2, comparable to that of Leu/Leu in NHERF-1.

3.5 Determinant NHERF residues for FERM binding

Based on our crystal structures, the binding affinities for several mutated NHERF-1 peptides were examined using surface plasmon resonance (SPR) measurements to identify determinant residues for the specificity (Table 3.6). The wild-type peptide binds the radixin FERM domain with extremely high affinity (K_d of 1.7 nM). We identified three nonpolar residues, Met346, Trp348 and Phe355, as the determinant residues (NHERF-1/M346, W348 and F355 in Table 3.3, respectively). The most important residue is Trp348, which makes both nonpolar and hydrogen bonding interactions as described above (Fig. 3.7b, c). Each mutation of these three residues reduces the binding affinity by from 25- to 33-fold, which corresponds to a loss in binding free energy of 8-9 kJ/mol. Compared with completely buried Trp348 and Phe355, Met346 is relatively exposed to solvent, while the contribution to the binding affinity is comparable to the two buried residues. This could be due to its role in stabilizing the N-terminal part of the NHERF

helix (Fig 3.5d). The next determinant residue was found to be C-terminal Leu358, the mutation of which resulted in 7-fold weaker binding. Leu354 at the molecular surface showed a relatively small contribution to the binding affinity (Fig 3.5b). These two residues of the NHERF-1 replace with Phe and Ile in NHERF-2. Alanine mutants of the Phe337 and Ile333 resulted in 4- and 3-fold weaker binding, respectively (Table 3.6). This may be because alanine replacement alone is not enough to completely abolish the side-chain contribution to the binding.

The contribution of two polar residues, Lys351 and Asn352, was found to be even smaller, where each mutation caused only a 2-fold reduction in the binding affinity. Contrary to this small contribution, the N-terminal basic region, which would be flexible but seems to interact with the acidic groove of the FERM domain (Fig. 3.6 *left*), was found to be important for strong binding of NHERF. Truncation of the N-terminal basic region resulted in a significant decrease (more than 50-fold) in the binding affinity (NHERF-1/C-term in Table 3.6). We failed to detect significant binding of the 13-residue N-terminal basic region of the NHERF-1 peptide in our SPR measurements (NHERF-1/N-term). This suggested dynamic properties of the ionic interaction between the N-terminal basic region and the FERM acidic groove. These observations are reminiscent of the flexible basic region of the ICAM-2 cytoplasmic tail, which aligned with the acidic groove of the FERM domain in the FERM-ICAM-2 complex and contributes to the strong binding (Hamada *et al.*, 2003).

The bifurcated hydrogen bonds formed by the C-terminal residue Leu358 are mediated by one oxygen atom of the terminal carboxylate group (Fig. 3.7b, c). The issue concerning whether the terminal carboxylate group is essential for peptide binding was examined using a peptide having three additional Ala residues at the C-terminus

(NHERF-1/C-AAA in Table 3.6). This replaces the negatively-charged carboxyl group with a peptide bond group to an Ala residue. It was found that the replacement reduced the binding affinity by 7-fold. The magnitude of this reduction was unexpectedly small. The modified peptide still exhibited high affinity for the FERM domain with a K_d value of 12 nM.

In conclusion, we propose Motif-2, a novel 13-residue FERM-binding motif with MDWxxxxx(L/I)Fxx(L/F). The key elements in this new motif are Met, Trp and Phe, which play a central role in nonpolar interactions with the FERM domain. The Asp residue is not involved in the intermolecular interaction but represents the N-terminal cap important for stabilizing the α-helix of the motif. The C-terminal Leu residue, which is replaced with Phe in NHERF-2, represents the next determinant residue. The other Leu residue, which is replaced with Ile in NHERF-2, has some significance in the binding. Finally, the N-terminal flanking basic region is essential for the strong binding. The unexpectedly small contribution of the carboxyl group of the C-terminal end residue implies that the FERM domain could bind Motif-2 located at loop regions of proteins other than the C-terminal regions.

3.6 Comparison with the moesin FERM-C-tail complex

The FERM domain of ERM proteins has been found to display multiple binding modes for target molecules (Fig. 3.9). The crystal structure of the moesin FERM domain bound to the C-tail domain has been reported (Fig. 3.9b) (Pearson *et al.*, 2000). The overall r.m.s deviation obtained from superposition of the moesin FERM domain with the radixin FERM domain bound to the NHERF-1 peptide is relatively large (0.88 Å) (Table 3.5). On pair-wise superposition of subdomain C, however, the deviation between subdomains C of

these complexes is smaller than those for superposition with free, Ins(1,4,5)P_3 and ICAM-2 bound form. The binding mode of the NHERF peptide helix is comparable to that of helix D of the C-tail domain of moesin. A superposition of the C-tail domain onto the FERM domain bound to the NHERF-1 peptide indicated significant overlap between these helices with a relatively small r.m.s. deviation (0.51 Å). This overlap of the binding regions clearly demonstrated the counteraction of the C-tail domain with the NHERF peptides for FERM binding (Fig. 3.10a). A structure-based comparison of the sequences, however, showed limited homology of the helices (Fig. 3.10b). In our SPR measurements, a 15-residue peptide encompassing the helix D residues exhibited no detectable binding to the FERM domain (Radixin/helix D in Table 3.6), while 28-residue peptide containing helix C and helix D (Radixin/C-term in Table 3.6) was found to have a K_d value of 72 nM. These results indicate that not only the helix D but also the upstream peptide region corresponding to helix C is necessary for FERM binding of the C-tail domain. The C-tail domain replaces two key residues, Met346 and Trp348, of NHERF with glycine and threonine, respectively, resulting in loosing extensive hydrophobic interactions (Fig. 3.10c, d). Alternatively, the C-tail domain replaces Asn352 of NHERF with an isoleucine residue, making hydrophobic contacts with the FERM domain. Ser356 of NHERF is replaced with glutamate, which forms an additional hydrogen bond with the FERM domain (Fig 3.10d). These alternative interactions enable both the helices displaying poor sequence homology to bind the same groove of subdomain C. Other interactions are basically common in the two helices and a comparison of all interactions is summarized in Fig. 3.10c, d.

3.7 Effects of PI (4, 5) P_2 binding on peptide bindings of the FERM domain.

Subdomains A and C of the FERM domain form the highly positively-charged surface

with a cleft for Ins(1,4,5)P_3 binding (Fig. 3.9a). This flat surface was proposed to associate plasma membrane (Hamada *et al.*, 2000). The PI(4,5)P_2-binding site is accessible even in the inactive closed form of ERM proteins, whereas the phosphorylation site is located at the interface inaccessible to protein kinase(s) without structural changes. PI(4,5)P_2 binding would open the structure, thus exposing both actin- and adhesion molecule–binding sites, as well as the site for phosphorylation, which subsequently stabilizes the open form. The proposed orientation of the FERM domain associated with the membrane also enables subdomains C and B to interact with the cytoplasmic tails of adhesion molecules (Hamada *et al.*, 2003). Similarly, in the proposed orientation, the NHERF-binding site at subdomains C and B is accessible to the NHERF tail. PI(4,5)P_2-mediated activation restricts ERM opening to the membrane. Adhesion molecules can then lock the ERMs at adhesion sites. The adhesion molecules, which contain positively charged regions just inside the cytoplasmic side of the membrane, may also recruit ERMs by pooling PI(4,5)P_2.

The PI(4,5)P_2 binding site of the FERM domain has no overlap with either NHERF or ICAM-2 binding site. Our SPR measurements showed that di-butanoyl- PI(4, 5)P_2 has no significant effect on the peptide bindings of the FERM domain even at an extremely high (50 μM -100 μM) concentration of this soluble PI(4,5)P_2 (Fig. 3.11a). Using PI(4,5)P_2 -containing lipid, PI(4,5)P_2/POPC (1:9), vesicles, PI(4,5)P_2 binding to the FERM domain was found to have a K_d value in the micromolar range (3.02 μM), which is much weaker than the peptide bindings (Fig. 3.11b). Similar affinity was also observed for PI(4,5)P_2 /POPC (3:7) vesicles. These results suggest that PI(4,5)P_2 binding does not interfere with the peptide bindings and the PI(4,5)P_2 -bound FERM domain could bind these target proteins.

3.8 Structural changes from the free- and the ICAM-2-bound forms

The binding site for the NHERF peptides does not really overlap with the ICAM-2-binding site (Fig. 3.9c, d). Nevertheless, the presence of two closely positioned peptide-binding sites displaying different target specificity implies that ERM targets from two different classes may compete for binding to endogenous ERM proteins and thereby modulate each other's function that require their binding to ERM proteins. Compared with the free form of the FERM domain, local but significant structural changes (the r.m.s. deviation of 1.08 Å) were found in subdomain C of the current NHERF-bound FERM domain (Fig. 3.12a). In comparison with the ICAM-2-bound FERM domain, we found larger structural changes (1.32 Å), which are induced by NHERF-1 binding to enlarge the β-sandwich groove (ca. 2 Å) with displacement of sheet β5C-β7C (Fig. 3.12b). Interestingly, this displacement is resulted in a narrowing of the groove between strand β5C and helix α1C, the major site for ICAM-2 binding (Hamada *et al.*, 2003) (Fig. 3.12b). This indicated that structural changes induced by NHERF binding might interfere with Motif-1 binding.

The induced-fit structural changes involve rearrangement of the side-chain packing of the β-sandwich and many small conformational changes of other residues in subdomain C. These changes seem to be initiated by the insertion of two hydrophobic residues, Phe355 and Trp348 of NHERF, into the hydrophobic pockets of the subdomain C. The side-chain phenyl group of Phe355 enlarges the pocket by pushing Phe267 and Phe269 of subdomain C (Fig. 3.12c). These displacements induce rotations of the side chains of Phe255 and Phe250. Simultaneously, Trp348 of NHERF pushes strands β6C and β7C by contacting two prolines, Pro259 and Pro265 of subdomain C, inducing rotation of the side chains of Leu225 and Ile248. These rearrangements of the side-chain packing permit sheet β5C-β7C to slide toward helix α1C without significant perturbation in the β-β

interactions within the sheet (Fig. 3.12c, d). Docking of Trp348 of NHERF into the pocket also induces a conformational change in loop β6C-β7C with a flip of the main chain of Asp261 by loosing the hydrogen bond with the main chain of Ala264.

3.9 Interference between Motif-1 and Motif-2 binding

Using the sensor chips, onto which cytoplasmic peptides of ICAM-2, ICAM-1, V-CAM-1 and CD44 were immobilized, SPR measurements were performed by injecting the purified radixin FERM domain with or without NHERF-1 peptide at different concentrations. It was found that NHERF-1 peptide reduced the amount of the FERM domain bound to the ICAM-2 peptide in a concentration-dependent manner (Fig. 3.13a). Previously, the C-terminal basic region of the ICAM-2 peptide has been shown to contribute to FERM binding by interacting with the acidic groove between subdomains B and C (Hamada *et al.*, 2003). Since the N-terminal flexible basic region of the NHERF-1 peptide also interacts with the same acidic groove, we speculated that the NHERF-1 peptide might directly compete with the ICAM-2 peptide for binding to the acidic groove. However, the N-terminal-truncated NHERF-1 peptide was found to interfere with FERM-ICAM-2 binding (Fig. 3.13b). Based on these binding experiments, we concluded that the binding of NHERF and ICAM-2 to the FERM domain is affected predominantly by induced-fit conformational changes in subdomain C. Similar results were obtained for the ICAM-1, V-CAM-1 and CD44 peptides that contain the Motif-1 sequences (Fig. 3.13c). Since the affinity of the FERM domain to these cytoplasmic peptides are weaker than that for ICAM-2 (Hamada *et al.*, 2003), the inhibitory effect of the NHERF-1 peptide on binding of these peptides are much larger (with a K_i value of ca. 50 nM). Therefore, we believe that NHERF-1 could displace most ERM-binding adhesion molecules from ERM proteins.

Figure 3.1 Crystals of the radixin FERM domain/NHERF complex

FERM/NHERF-1 complex

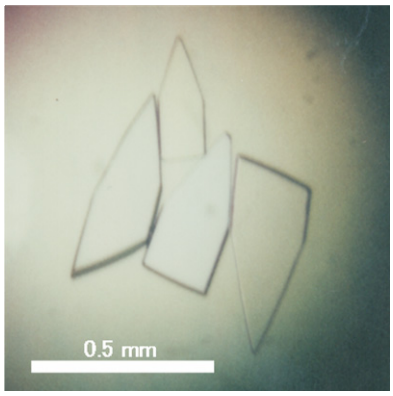

Crystallization condition		
Drop:	FERM	0.33 mM
	NHERF-1	0.33 mM
Reservoir:		10% 2-propanol
		20% PEG4000
		0.1M HEPES-Na pH 7.5
Temperature:		4 degree

FERM/NHERF-2 complex

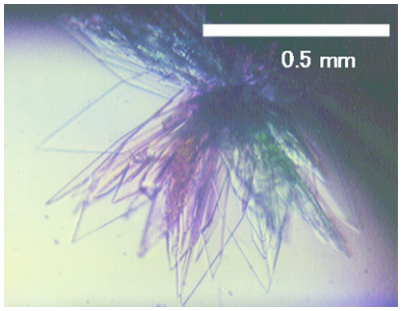

Crystallization condition		
Drop:	FERM	0.45 mM
	NHERF-2	0.45 mM
Reservoir:		5% 2-propanol
		10% PEG4000
		0.1M HEPES-Na pH 7.5
Temperature:		4 degree

Table 3.1 Crystallographic data

		FERM/NHERF-1	FERM/NHERF-2
Space group		$P2_12_12_1$	$P2_12_12_1$
Cell dimensions (Å)	*a*	69.38	68.63
	b	146.27	144.37
	c	177.76	177.94
Resolution (Å)		30-2.5	30-2.8
Reflections:	Measured	459178	118827
	Unique	62668	41789
Completeness (%)[b]		99.2/98.9	95.0/95.0
R_{sym}[a] (%)[b]		6.5/34.9	8.5/31.7
Mean I/σ[b]		10.5/2.1	11.6/2.8

[a] $R_{sym} = \Sigma| I - < I > | / \Sigma I$; calculated for all data.

[b] Each pair of values are for overall / outer shell. The resolution ranges of their outer shells are 2.64-2.50 Å (NHERF-1) and 2.90-2.80 Å (NHERF-2).

Table 3.2 Solutions of the rotation function and translation function

FERM/NHERF-1 complex

	α	β	γ	X	Y	Z	C (I)	R
Mol_A	157.8	90.00	244.2	0.129	0.469	0.165	14.6	53.1
	24.60	86.66	65.40	0.370	0.471	0.336	11.7	54.1
	78.10	85.48	62.81	0.105	0.337	0.196	11.6	54.0
Mol_B	78.10	85.48	62.81	0.604	0.337	0.196	28.5	49.4
	115.2	85.68	63.48	0.296	0.827	0.083	28.4	49.5
	169.46	83.79	66.59	0.086	0.418	0.945	24.5	50.9
Mol_C	115.20	85.68	63.41	0.296	0.827	0.083	46.3	43.4
	169.5	83.79	66.59	0.086	0.418	0.945	41.9	45.3
	58.20	90.00	241.7	0.704	0.331	0.416	32.6	48.5
Mol_D	169.5	83.79	66.59	0.086	0.419	0.945	58.3	38.7
	16.80	90.00	244.8	0.927	0.920	0.554	46.6	49.5
	157.8	90.00	244.2	0.128	0.470	0.164	45.6	44.0

FERM/NHERF-2 complex

α	β	γ	X	Y	Z	C (I)	R
126.4	91.95	208.7	0.121	0.388	0.317	75.6	31.5
1.62	80.18	210.7	0.398	0.312	0.188	45.5	52.3
35.08	80.36	210.99	0.022	0.307	0.658	45.4	52.6

This table includes the top three of the molecular replacement solutions sorted by the correlation coefficient C(I) values which are calculated using intensity and R-factor (R) for $P2_12_12_1$. The (α, β, γ) are Eulerian angles and (X, Y, Z) are the fractional coordinates of the unit cell axes. These calculations used the reflections between 3-6 Å and the radius of integration is 20 Å. Both crystals contain four complexes per asymmetric unit. The most probable solutions are highlighted by blue boxes.

Table 3.3 Refinement statistics

		FERM/NHERF-1	FERM-NHERF-2
Resolution range (Å)		30.0-2.5	30.0-2.8
Number of residues:	protein	1.186	1.176
	peptide	80	70
Atoms included	protein	9824	9805
	peptide	588	638
	water	617	163
R_{cryst}-factor/R_{free}-factor(%) [a]		22.9/26.7	22.1/27.9
Meam B-factor (Å^2)	overall	38.4	36.4
	protein	36.5	35.0
	peptide	71.1	60.2
	water	38.5	27.1
Rms deviations [b]		0.007 Å, 0.97°	0.008 Å, 1.05°

[a] R_{cryst} and $R_{free} = \Sigma \parallel F_o \mid - \mid F_c \parallel / \Sigma \mid F_o \mid$, where the free reflections (2.5% of the total used) were held aside for R_{free} throughout refinement.

[b] Two values are for bond lengths, bond angles, respectively.

FERM/NHERF-1 complex

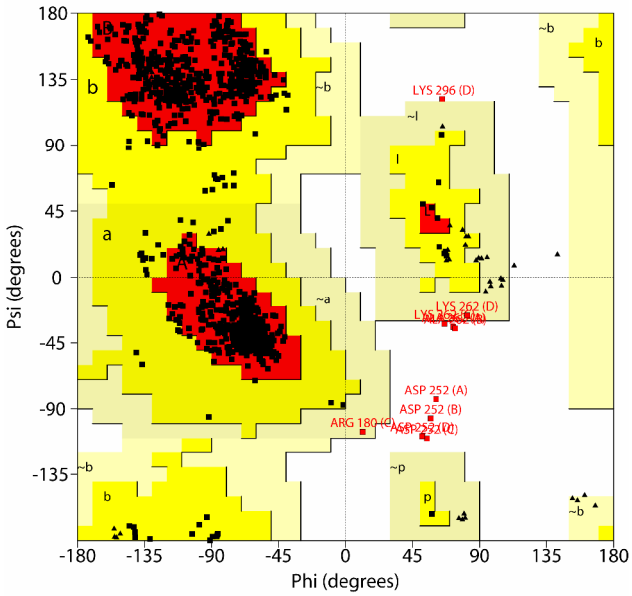

FERM/NHERF-2 complex

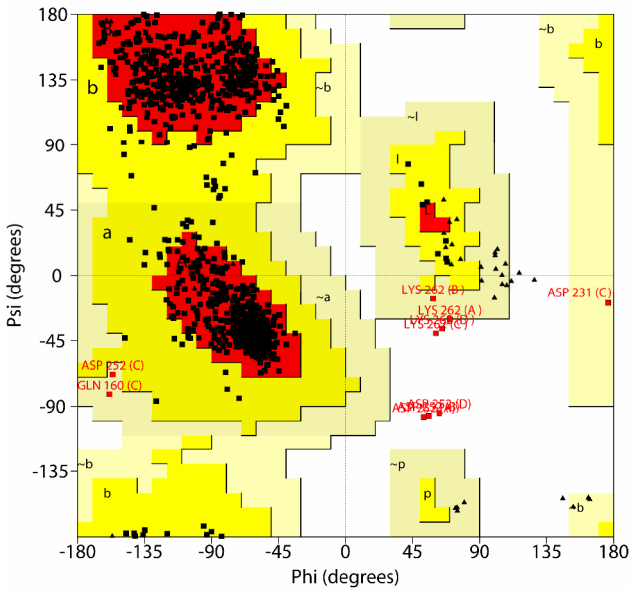

Figure 3.2 Ramanchandran plots of the FERM/NHERF complexes

Main-chain conformational angles were analyzed using the *PROCHECK* software. The Φ angle around the N-Cα bond is indicated on the horizontal axis and the Ψ angle around the Cα-C bond is indicated on the vertical axis. Glycine residues are shown as triangle, the other residues are shown squares. Most favored, additional allowed generously allowed regions are shaded in black, and disallowed regions are in red. The labels of "a" indicate the regions for α-helix, "b" for β-strand, and "l" for α_L-helix. In the plots, residues 252 and 262 of both complexes are in disallowed region.

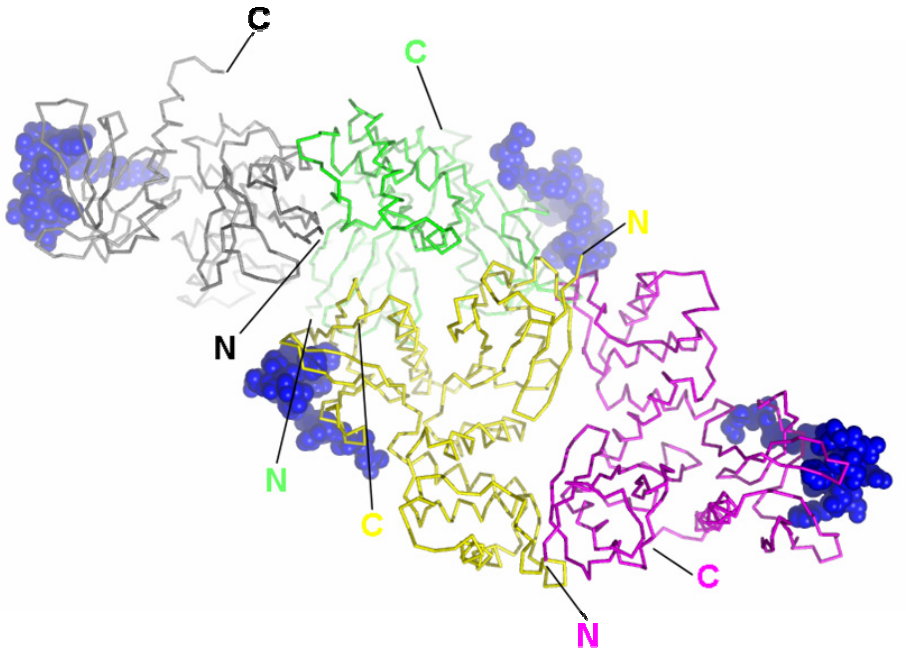

Figure 3.3 Structure of the radixin FERM domain bound to the NHERF-1 peptide in asymmetric unit.

C_α trace ribbon models and space-filled models show the radixin FERM domains and the NHERF-1 peptides, respectively.

Table 3.4 Comparison of the FERM domains in asymmetric unit.

Chain	FERM/NHERF-1	FERM/NHERF-2
A-B	0.36	0.39
A-C	0.26	0.34
A-D	0.42	0.38
B-C	0.31	0.38
B-D	0.37	0.46
C-D	0.35	0.36

The r.m.s deviations obtained from superposition of the FERM domains in the asymmetric unit are shown in this table. Average r.m.s deviation of both complexes is less than 0.4 Å.

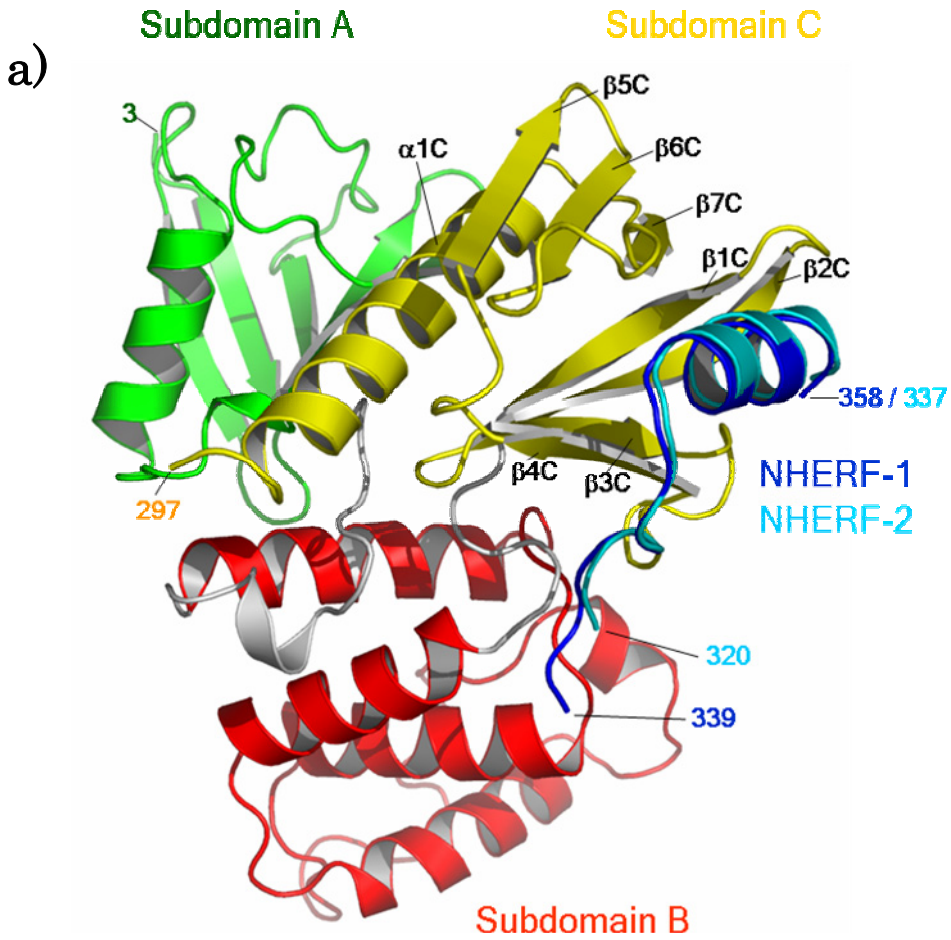

Figure 3.4 a) Overall structure of the Radixin FERM domain bound to NHERF peptide. Ribbon representations of the radixin FERM domain bound to the NHERF-1 (blue) and NHERF-2 (light blue) peptide. The radixin FERM domain consists of subdomains A (the N-terminal 82 residues in green), B (residues 96-195 in red), and C (residues 204-297 in yellow).

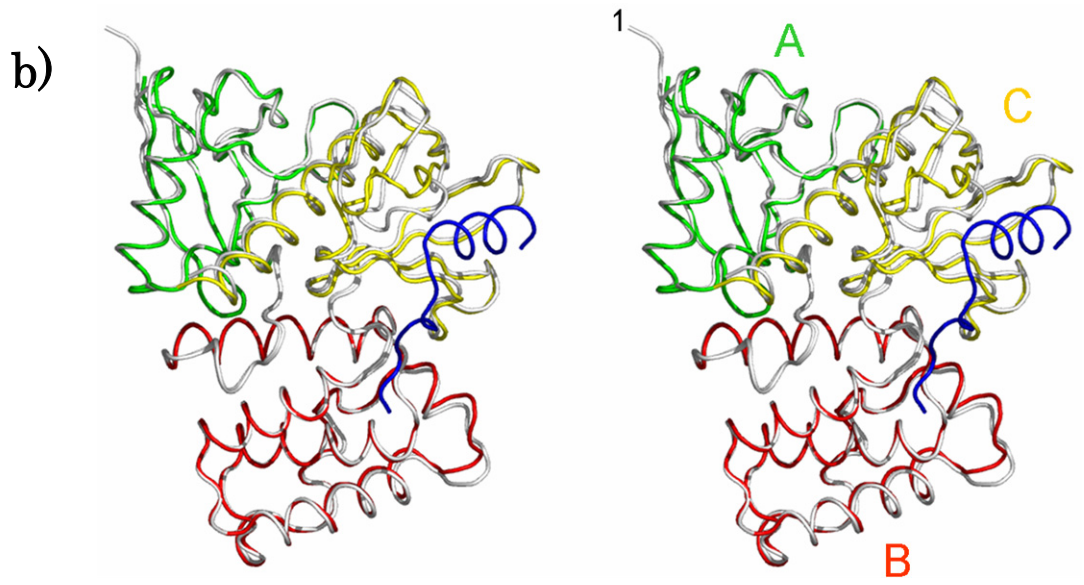

Fig 3.4 b) Superposition of the NHERF bound form with free form.

Superposition of the NHERF bound form with free form in stereo view is shown. Color of the FERM-NHERF complex is same in Fig 3.4a. The free form colored white.

Table 3.5 Comparison of the NHERF bound form with other molecules bound forms.

Residues	Free form	IP3 bound	ICAM-2 bound	C-tail bound
3-297	0.96	0.95	1.48	0.88
3-203	0.66	0.67	0.92	0.82
96-297	1.03	1.04	1.29	0.95
3-95	0.46	0.49	0.85	0.42
96-203	0.68	0.69	0.36	0.77
204-297	1.08	1.06	1.32	0.76

The r.m.s deviations obtained from superposition of the FERM domains in the NHERF bound form with in the free and other molecule-bound forms were shown in this table. Superposition of subdomain C (204-297) or subdomain C containing regions (3-297, 96-297) resulted in relatively large r.m.s deviations.

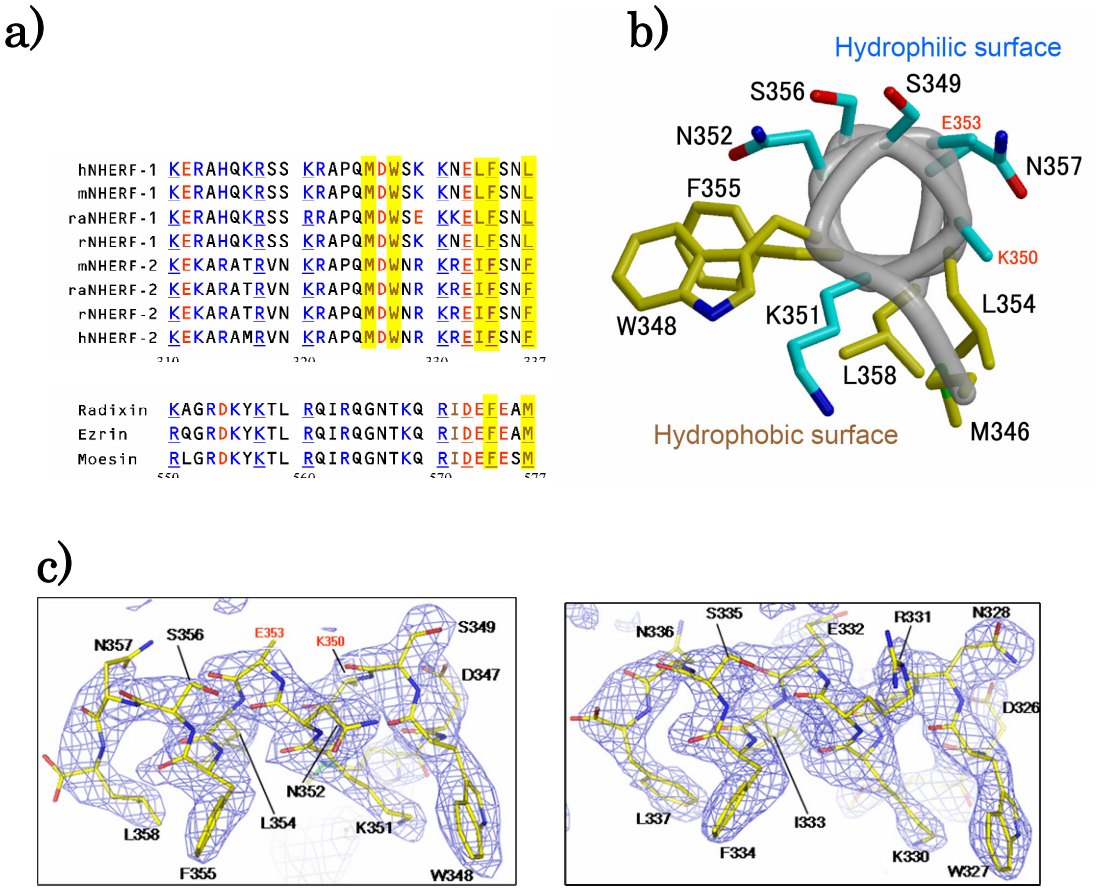

Figure 3.5 Structure of the NHERF peptide.

a) Peptides synthesized based on the sequence of the NHERF-1 and -2 tails were used for the structural work. The 28-residue NHERF peptides consist of the N-terminal polar region (basic residues in blue) and the C-terminal amphipathic region (nonpolar residues in brown). The 20 residues (339-358) of the NHERF-1 peptide defined on the current map display a N-terminal loop (residues 339-347) followed by an α helix consisting of the extreme C-terminal 11 residues (348-358). Key residues involved in binding to the radixin FERM domain are in bold and highlighted in yellow (see text). Conserved residues between NHERF peptides and the C-terminal tail of ERM proteins are underlined.**b)** A helical projection of the C-terminal helix of the NHERF-1 peptide found in the FERM-NHERF-1 complex crystal. The side chains are shown as stick models in yellow (non-polar residues) and cyan (polar). The poorly-defined side chains of K350 and E353 (smaller red labels) are omitted. Omit electron density maps for the NHERF peptides. **c)** The C-terminal helices of NHERF-1 (left) and -2 (right) bound to the hydrophobic groove of the radixin FERM domain are shown with stick models with omit electron density maps countered at 1σ level.

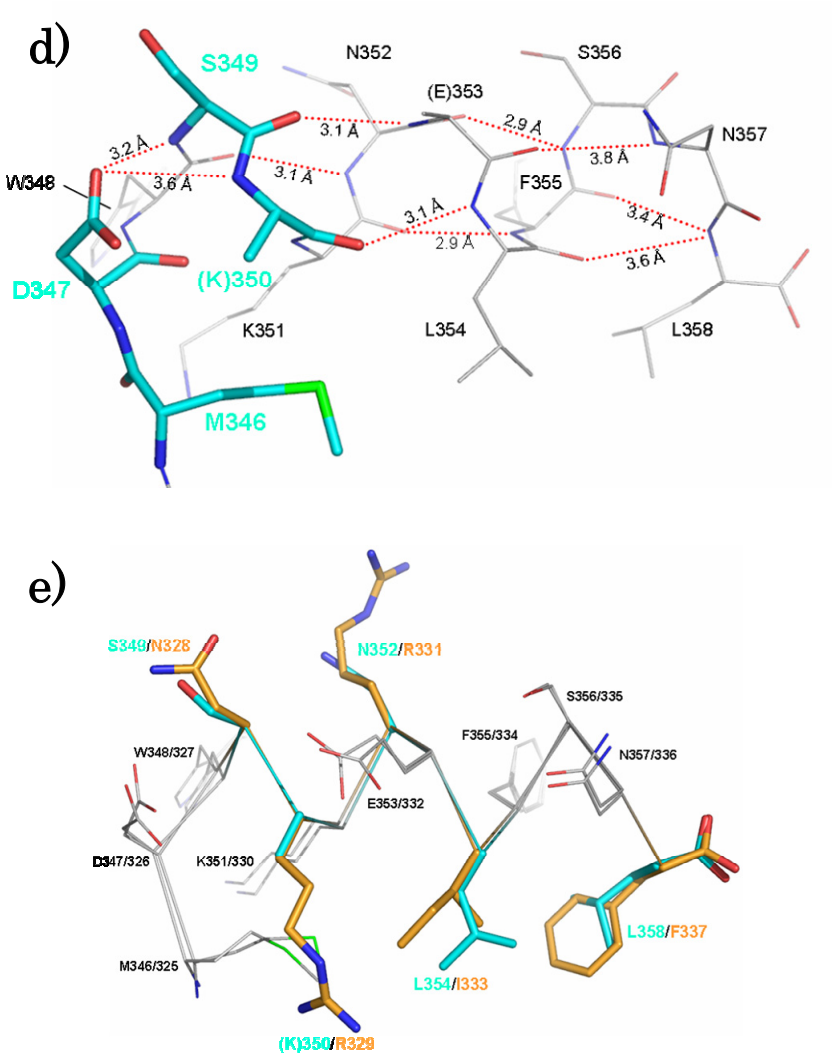

Figure 3.5 (*continue*)

d) The N-terminal capping structure of the NHERF-1. The peptide structure of the NHERF-1 (346-358) is shown stick-models. The red doted lines show hydrogen bonds. The side chain of the D347 residue forms the N-terminal cap of α-helix by hydrogen bonding to the main-chain amide group(s) of S349 and/or K350. The aliphatic side-chain of the M346 stabilizes the N-terminal cap by associating with the aliphatic side-chain of the K351 and main-chain C_α of the K350. **e)** Comparison of the C-terminal helices of NHERF-1 and NHERF-2. The replaced residues between NHERF-1 and NHERF-2 are shown cyan and brown, respectively. The C-terminal L residue, which is replaced with Phe in NHERF-2 and the other Leu residue, which is replaced with Ile in NHERF-2, has some significance in the binding.

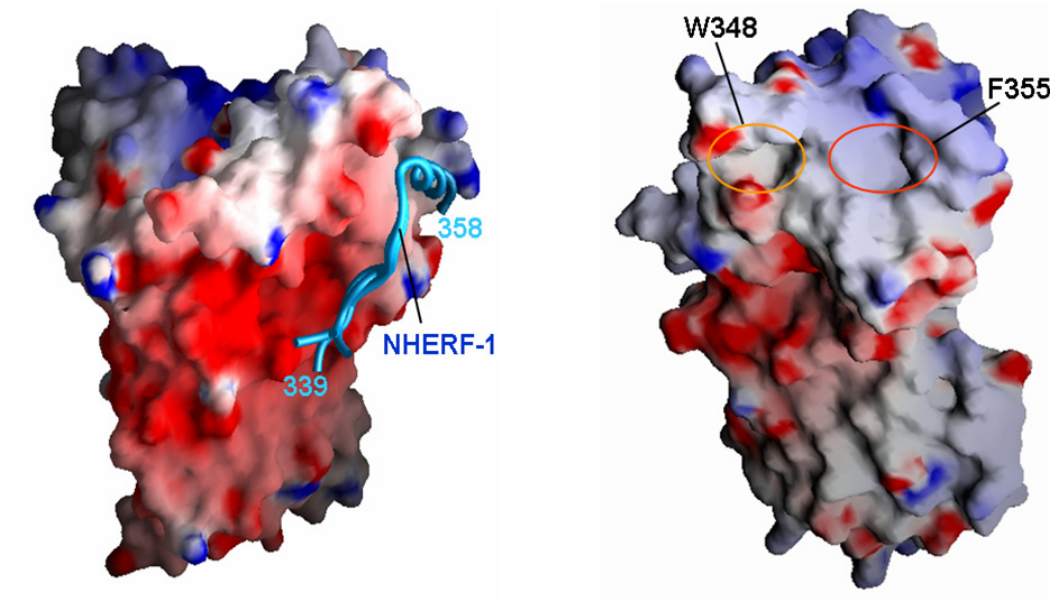

Figure 3.6 Electrostatic molecular surface of the NHERF-1 binding site.

Front- (*left*) and side- (*right*) views of surface electrostatic potentials of the radixin FERM domain. The front-view is viewed from the same direction as in **Fig. 3.2**. Positive (blue, +14 kT/e) and negative (red, -14 kT/e) potentials are mapped on the van der Waals surfaces. The four crystallographic-independent NHERF-1 peptides are shown in tube models (cyan). A side-view of the FERM domain is shown without the NHERF-1peptide to show the two pockets for the Trp348 and Phe355 side chains from the NHERF-1 peptide.

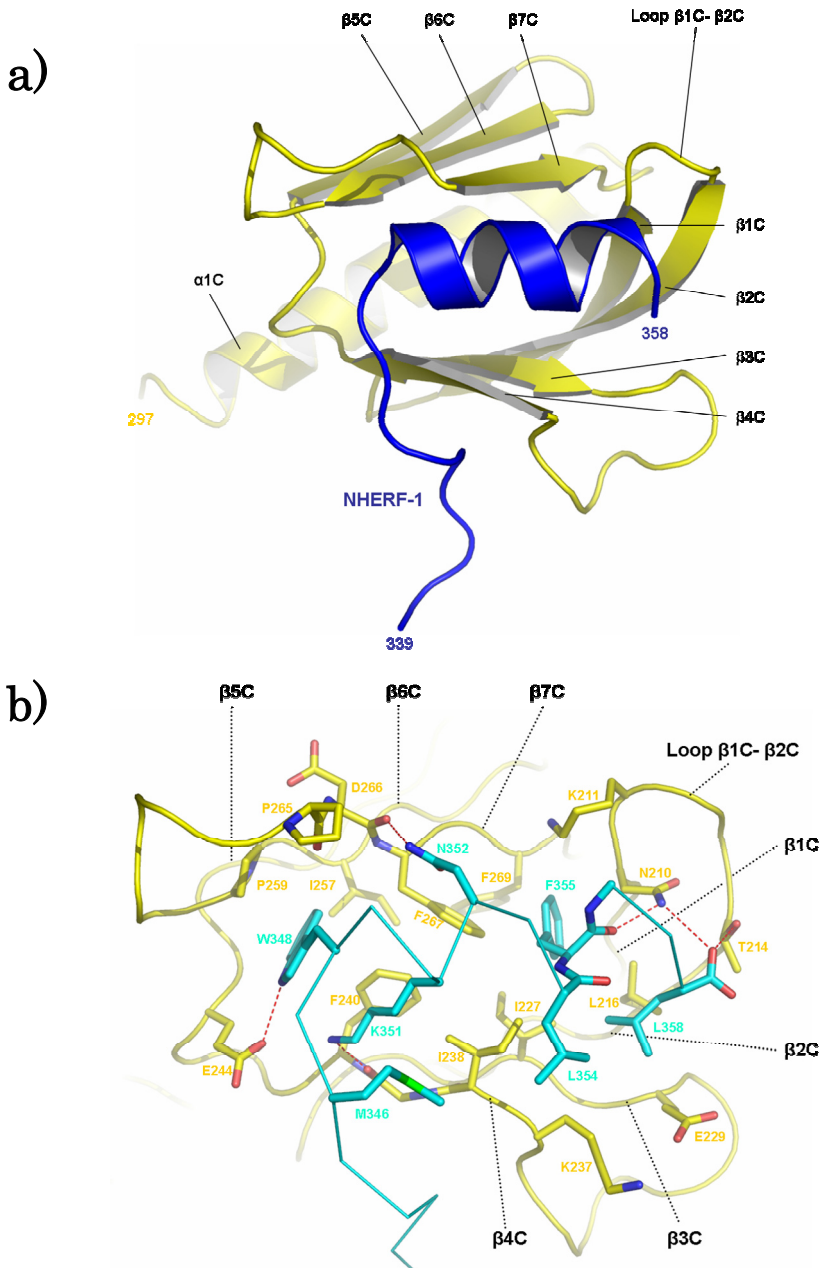

Figure 3.7 Interaction of the FERM domain-NHERF-1.

a) The interaction between subdomain C and the NHERF-1 peptide. The NHERF-1 peptide is shown as a ribbon model (blue). **b)** A close-up view of the amphipathic helix of NHERF-1 peptide (cyan) docked to the groove formed by the β-sandwich of subdomain C (yellow). Hydrogen bonds are shown with dotted lines. The C-terminal carboxyl group of Leu358 is labeled with CPX. The aromatic rings from Trp348 and Phe355 are docked to the pockets.

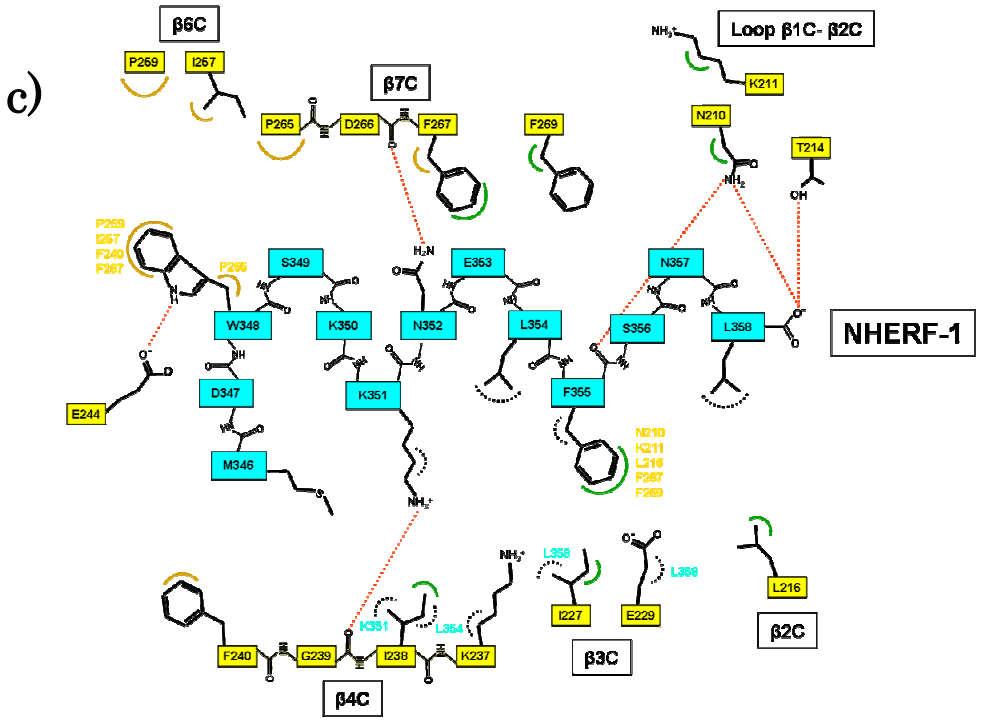

Figure 3.7 (*continue*)

c) Schematic representation of the interaction between subdomain C and NHERF-1 peptide. The NHERF-1 peptide is shown in cyan, subdomain C in yellow. Red dotted lines represent hydrogen bonds. Semicircle represents hydrophobic interactions.

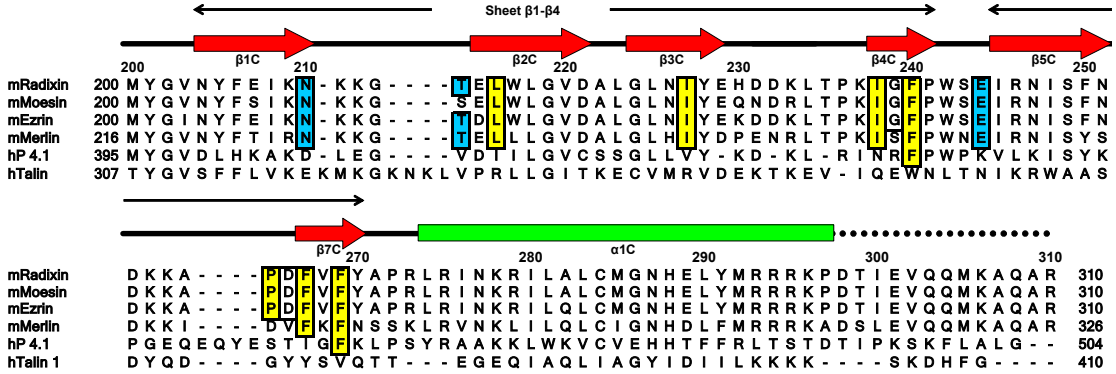

Figure 3.8 Sequence alignments of subdomain C from related FERM domains.

The FERM subdomain C of mouse radixin, ezrin, moesin and human band 4.1 (hP 4.1) and talin (hTalin) are aligned with the secondary structure elements of the radixin FERM subdomain C at the top: α helix (a green rectangle) and β strands (red arrows). Boxed residues participate in nonpolar (highlighted in yellow) and polar (blue for side-chain and white for main-chain) interactions with the NHERF-1 peptide. Mouse FERM domains exhibit 100% sequence identity with those of human.

Table 3.6 Binding affinities of the NHERF-1 peptides for the radixin FERM domain.

Peptide[a]	Sequence[b]	K_d (nM)[c]	K_d (m) / K_d (w)
Residue number	331 341 351 358		
	.---------.---------.--------		
xtal/visible	----------KRAPQMDWSKKNELFSNL		
NHERF-1/wild	KERAHQKRSSKRAPQMDWSKKNELFSNL	1.69±0.4	1.00
NHERF-1/K351	KERAHQKRSSKRAPQMDWSK**A**NELFSNL	3.08±1.0	1.82
NHERF-1/N352	KERAHQKRSSKRAPQMDWSKK**A**ELFSNL	3.19±1.3	1.89
NHERF-1/L354	KERAHQKRSSKRAPQMDWSKKNE**A**FSNL	4.95±0.6	2.92
NHERF-1/L358	KERAHQKRSSKRAPQMDWSKKNELFSN**A**	11.9±3.0	7.04
NHERF-1/M346	KERAHQKRSSKRAPQ**A**DWSKKNELFSNL	42.9±6.2	25.4
NHERF-1/F355	KERAHQKRSSKRAPQMDWSKKNEL**A**SNL	45.2±6.0	26.7
NHERF-1/W348	KERAHQKRSSKRAPQMD**A**SKKNELFSNL	56.5±6.9	33.4
NHERF-1/WKF	KERAHQKRSSKRAPQMD**A**SK**A**NEL**A**SNL	-	
NHERF-1/N-term	KERAHQKRSSKRA	-	
NHERF-1/C-term	AAAPQMDWSKKNELFSNL	92.5±0.3	54.7
NHERF-1/C-AAA	KERAHQKRSSKRAPQMDWSKKNELFSNL**AAA**	12.0±1.1	7.1
Radixin/helix D	RQGNTKQRIDEFEAM	-	
Radixin/C-term	KAGRDKYKTLRQIRQGNTKQRIDEFEAM	71.7±1.02	42.3
NHERF-2/Wild	KEKARAMRVNKRAPQMDWNRKREIFSNF	9.52±0.01	1.00
NHERF-2/I333	KEKARAMRVNKRAPQMDWNRKRE**A**FSNF	26.7±0.14	2.80
NHERF-2/F337	KEKARAMRVNKRAPQMDWNRKREIFSN**A**	40.4±0.20	4.24
NHERF-2/C-term	AAAPQMDWNRKREIFSNF	96.8±0.62	57.3

[a]The peptides are for the juxta-membrane regions of human NHERF-1 (residues 331-358) and its mutation and deletion peptides. Mutated alanine residues in the NHERF-1 peptides are shown in bold. [b]Determinant residues in the FERM-binding peptides are boxed. [c]The obtained K_d values with their standard deviations. All measurements were performed at 25˚C in HBS-EP buffer containing 10 mM Hepes-Na (pH 7.4), 150 mM NaCl, 1 mM EDTA, 1 mM DTT, and 0.05% surfactant P20.

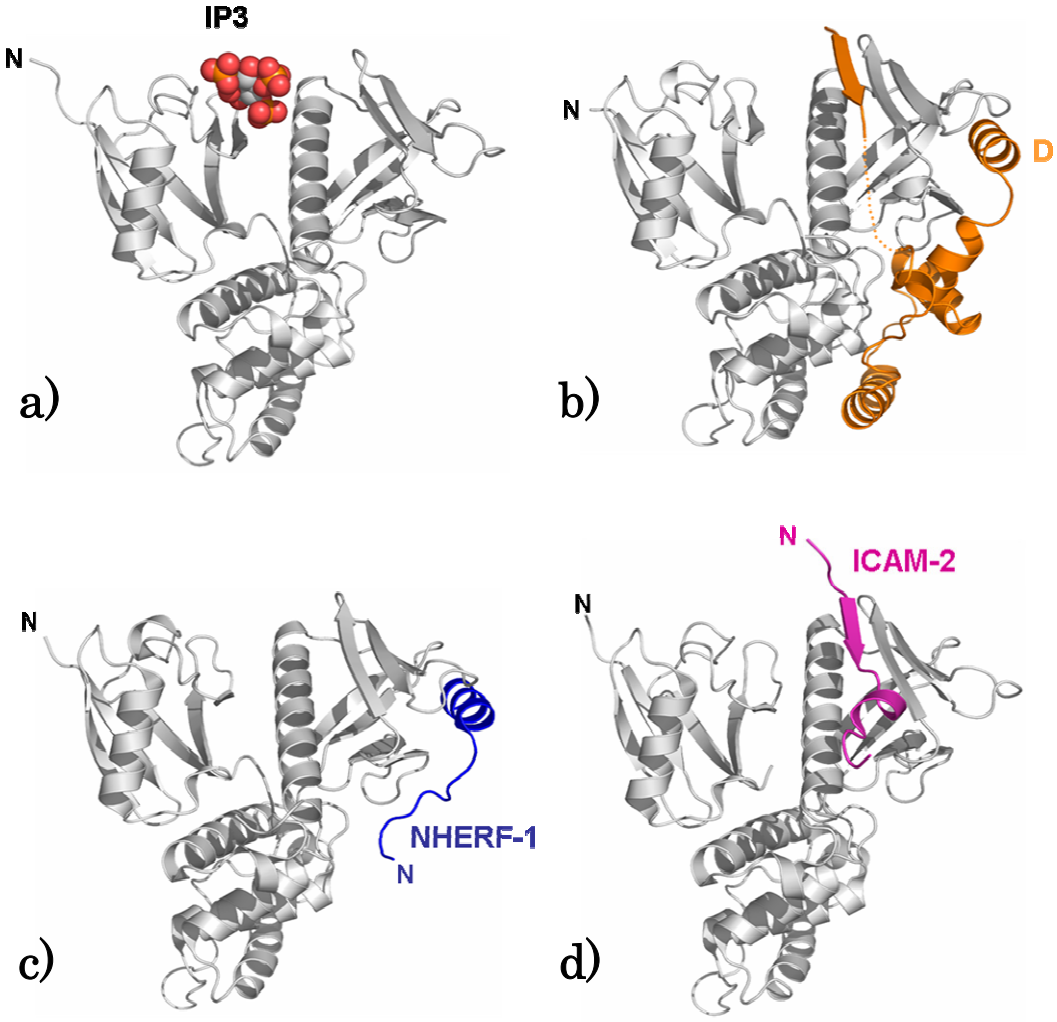

Figure 3.9 Multi-binding modes found in the FERM domain of ERM proteins.

a) The radixin FERM domain (gray) complexed with Ins(1, 4, 5) P_3 (Hamada *et al.*, 2003), which is shown as a space-filled model.

b) The moesin FERM domain complexed the C-tail domain (orange) (Pearson *et al.*, 2000).

c) The radixin FERM domain complexed with the NHERF-1 peptide (blue).

d) The radixin FERM domain complexed with the ICAM-2 cytoplasmic peptide (magenta) (Hamada *et al.*, 2003).

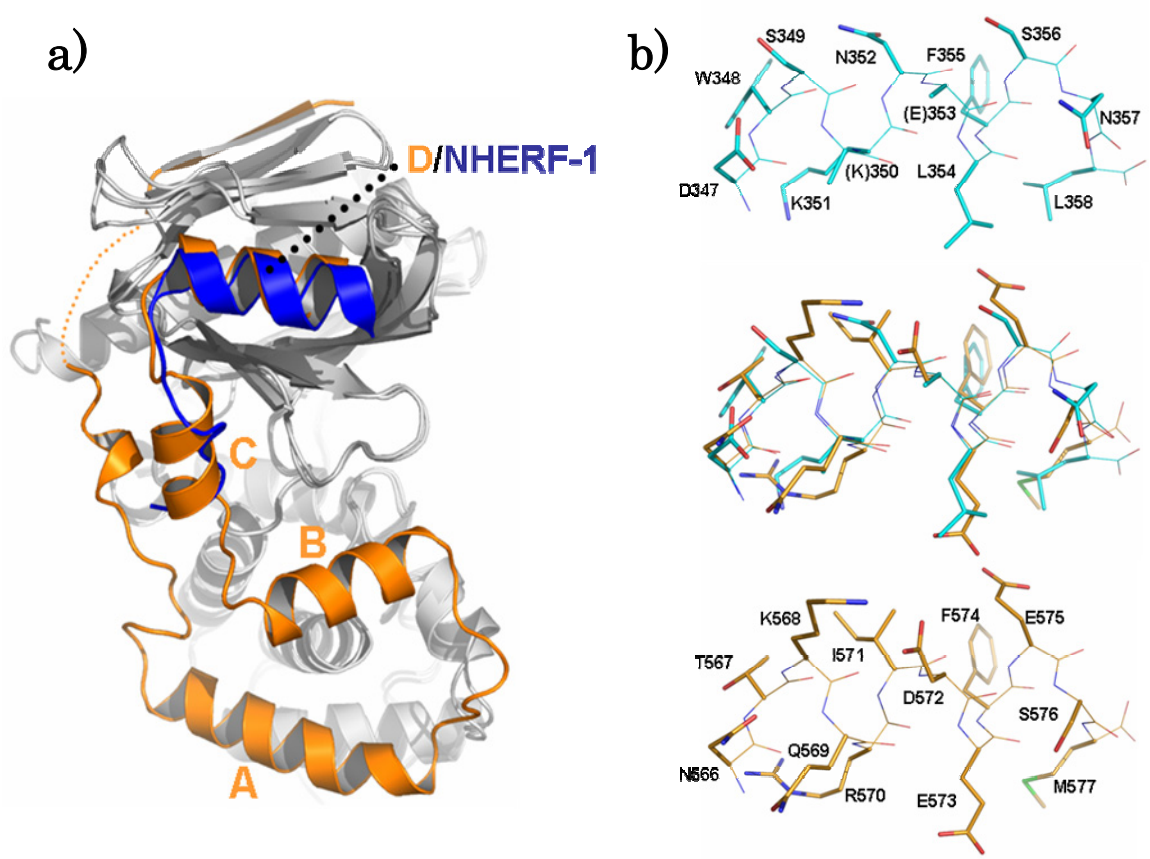

Figure 3.10 Comparison of the NHERF-1 with α-helix D of the C-tail domain.

a) Superposition of the FERM domain in the radixin FERM-NHERF-1 complex and the moesin FERM-C-tail complex is shown. The NHERF-1 peptide is blue, the moesin C-terminal domain is brown and both FERM domains are grey. The moesin C-terminal domain is composed of four α-helix (A-D). Helix D masks the NHERF-1 binding site.

b) Comparison of the C-terminal helix D of the NHERF-1 peptide (cyan) bound to the radixin FERM domain and helix D of the moesin C-terminal domain (brown).

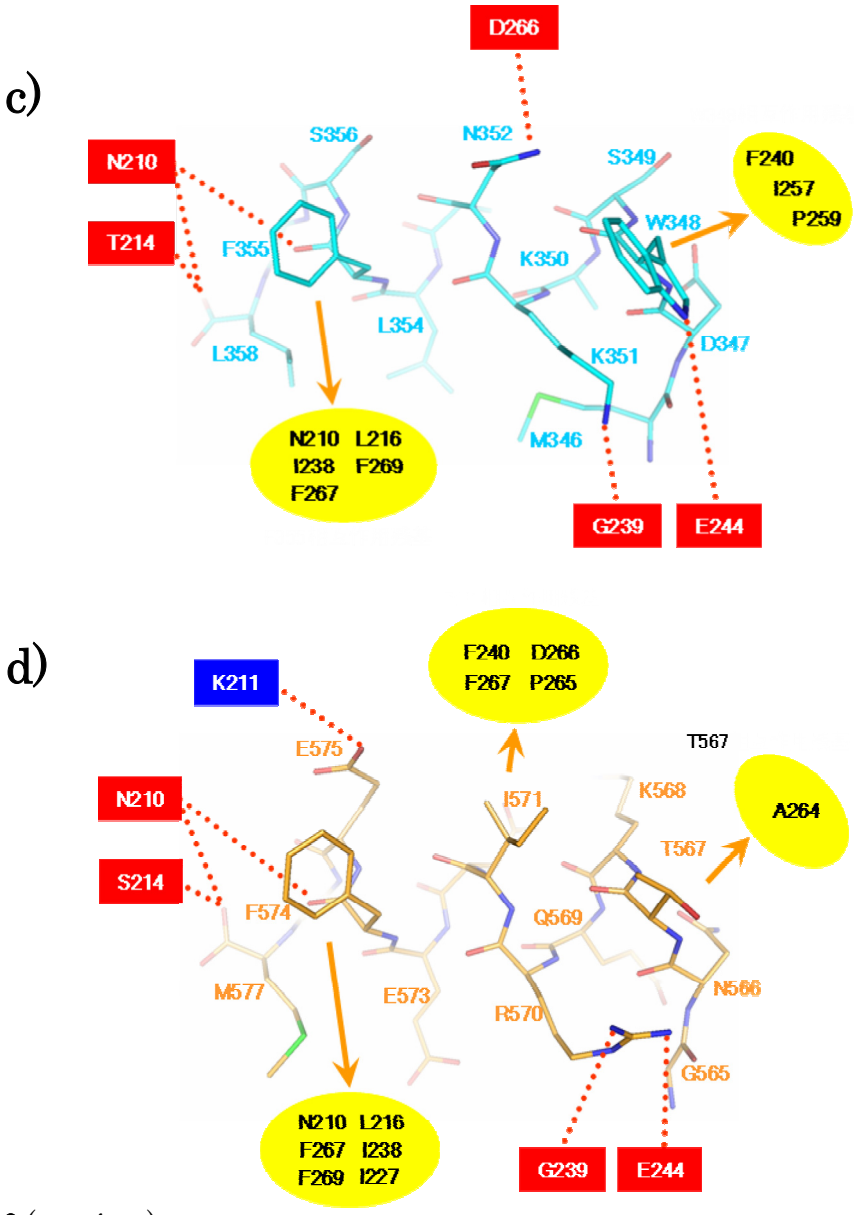

Figure 3.10 (*continue*)

Binding of the NHERF-1 peptide to the radixin FERM domain (**c**) is compared with that of the C-tail domain to the FERM domain found in the moesin masked form (**d**). Met346 and Trp348 of NHERF are replaced with threonine and glycine in the C-tail domain. Alternatively, Asn352 of NHERF is replaced with isoleucine, making hydrophobic contacts with the FERM domain. Ser356 of NHERF is replaced with glutamate, which forms an additional hydrogen bond with Lys211 of the FERM domain. Lys351 of NHERF is homologically replaced with arginine, which forms two hydrogen bonds with the FERM domain, the main chain of Gly239 and the side chain of Glu244. The former hydrogen bond is common and the latter one is corresponding to that to Trp348 of NHERF.

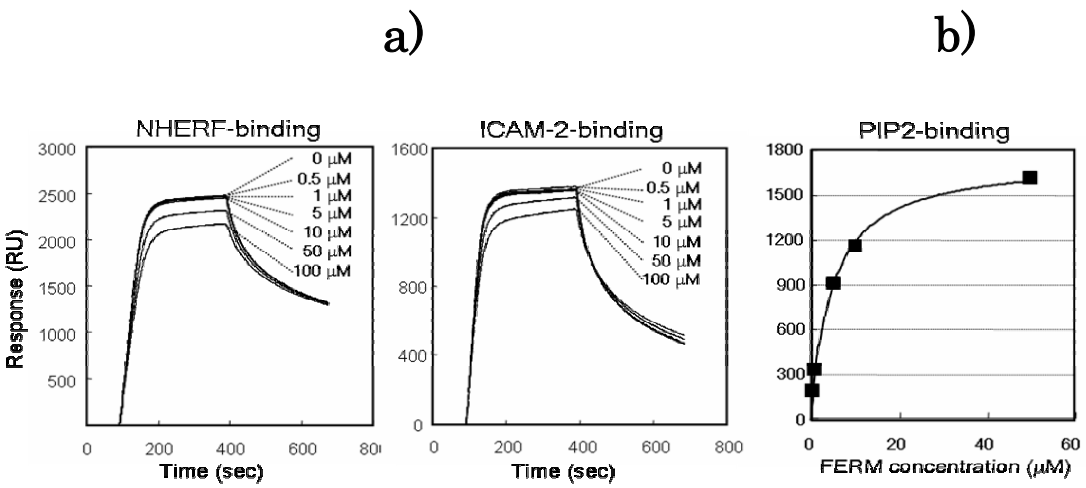

Figure 3.11 Effects of PI (4, 5) P_2 binding on peptide bindings of the FERM domain.

(**a**) Sensor diagrams obtained from SPR measurements with the NHERF-1 (*left*) or ICAM-2 (*right*) peptide immobilized to the sensor chip. Purified radixin FERM domain (100 nM) was injected into the sensor chips with or without soluble di-butanoyl- PI (4, 5) P_2, of which concentrations are indicated (0 μM – 100 μM). The NHERF-1 peptide is the same as that used in the structural work. The ICAM-2 peptide is the full-length cytoplasmic tail (residues 250-277: HRRRTGTYGVLAAWRRLPRAFRARPV).

(**b**) Binding isotherm for the radixin FERM domain and POPC/ PI (4, 5) P_2 (9:1) vesicles from equilibrium SPR measurements. The K_d value (3.02 ±1.11 μM) was obtained from the theoretical fitted curve (a solid line).

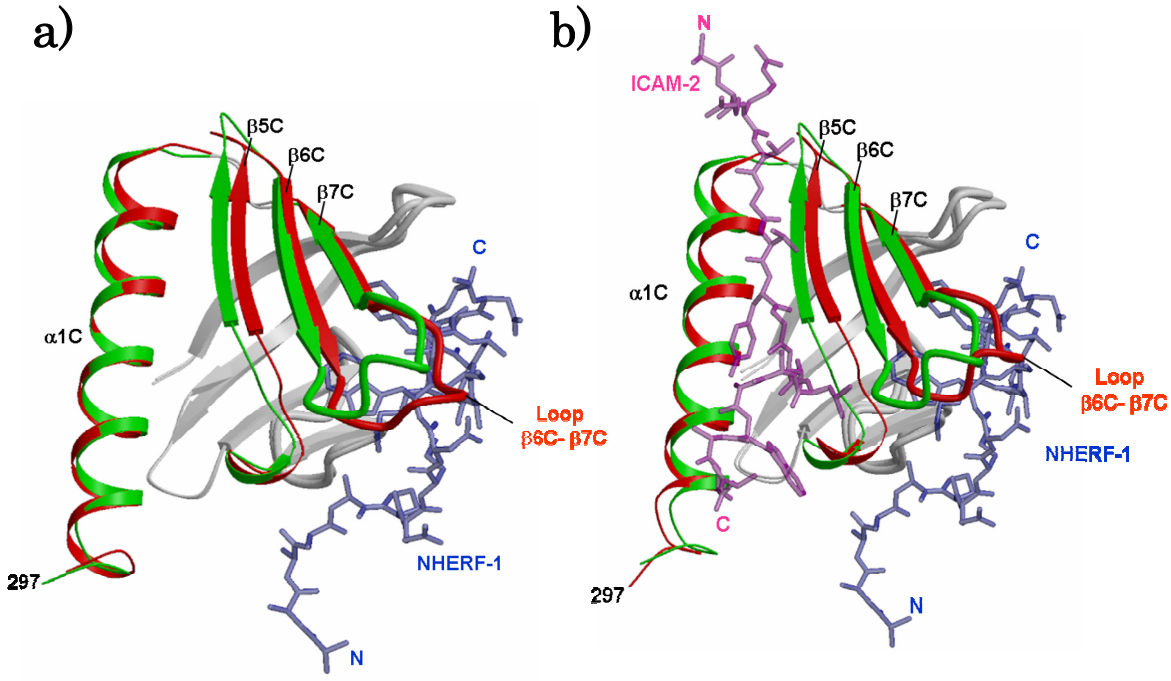

Figure 3.12 Induced-fit structural changes in subdomain C cause interference between Motif-1 and Motif-2 binding to the FERM domain.

a) Front-view of superposition of subdomain C in the free and NHERF-1-bound forms. The NHERF-1 peptide (blue) is shown as a stick model. Loops are colored in green (NHERF-1-bound form) and red (free form). Two structures are superimposed using helix α1C and sheets β1C-β4C. These secondary structures display minimum deviations of the mutual positions. **b**) Front-view of the superposition of subdomain C in the NHERF-1- and ICAM-2-bound forms. The NHERF-1 (blue) and ICAM-2 (pink) peptides are shown as stick models. Helix α1C and sheet β5C-β7C are colored in green (NHERF-1-bound form) and red (ICAM-2-bound form).

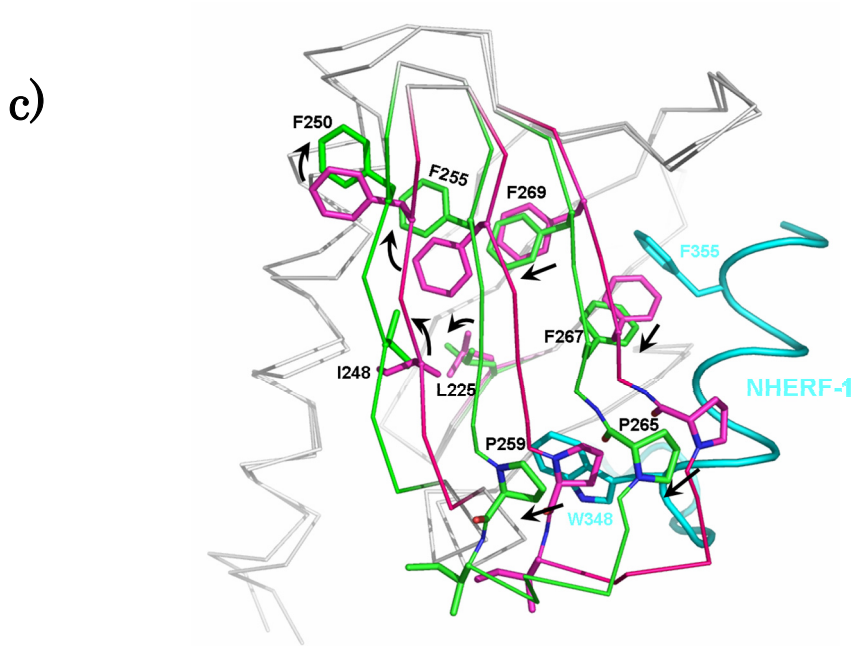

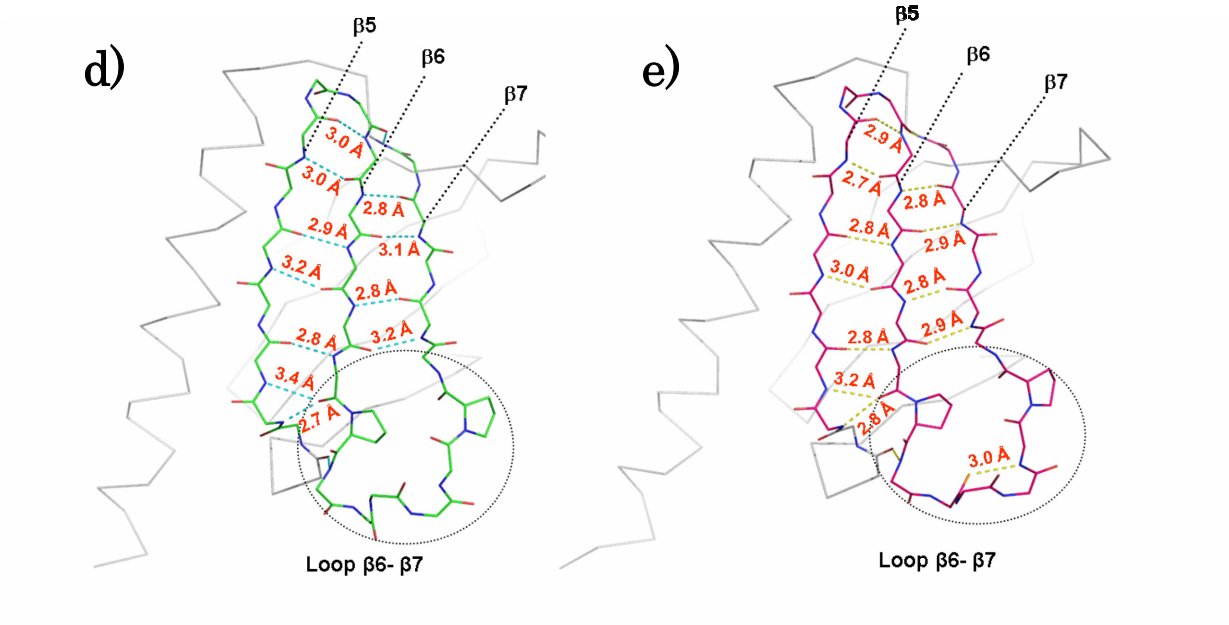

Figure 3.12 (*continue*) **c)** Rearrangement of the side chain packing of Subdomain C. Sheet ß5C-ß7C is colored in green (NHERF-1 bound form) and red (ICAM-2 bound form). d) The ß-ß interactions in subdomain C of the NHERF bound form. Hydrogen bonds are shown with broken line. e) The ß-ß interactions in subdomain C of the ICAM-2 bound form.

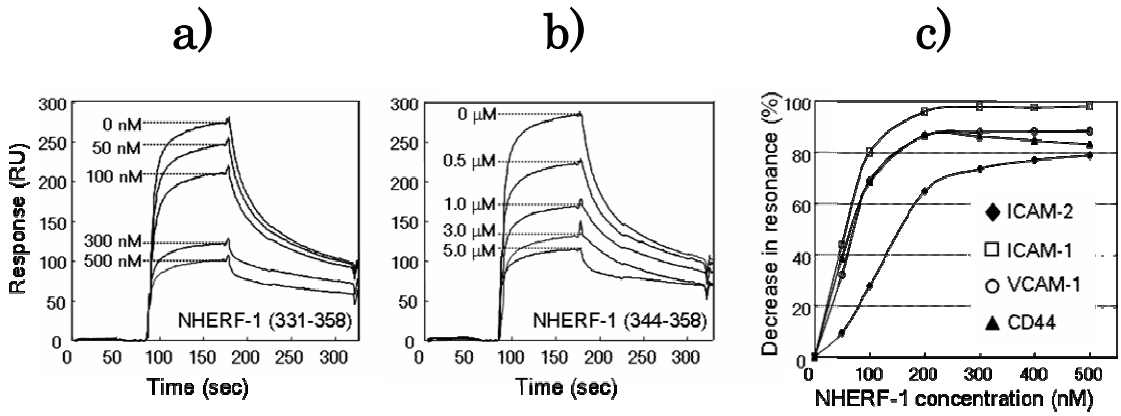

Figure 3.13 Interference between motif-1 and motif-2 binding.

a) Sensor diagrams obtained from SPR measurements with the ICAM-2 peptide immobilized to the sensor chip. Purified radixin FERM domain (100 nM) was injected into the sensor chips with or without the NHERF-1 peptide used for the structural work. The concentrations of the NHERF-1 peptide are indicated. **b)** Sensor diagrams obtained from SPR measurements with the ICAM-2 peptide immobilized to the sensor chip. Purified radixin FERM domain (100 nM) was injected into the sensor chips with or without the N-terminal truncated NHERF-1 peptide (residues 344-358). **c)** Summary of SPR analyses of the binding of the FERM domain to several cytoplasmic tail peptides immobilized onto sensor chips. The observed decreases (%) in resonances were plotted against NHERF-1 concentration. The peptides are for the juxtamembrane regions of mouse adhesion molecules having Motif-1 that binds the radixin FERM domain (Hamada *et al.*, 2003); ICAM-2 (the same as in Fig. 3.9a),
CD44 (584-620: NSRRRCGQKKKLVINGGNGTVEDRKPSELNGEASKSQ), ICAM-1 (483-510: QRKIRIYKLQKAQEEAIKLKGQAPPP) and
VCAM-1 (720-739: ARKANMKGSYSLVEAQKSKV).

4, Discussion

4.1 The FERM-NHERF interaction

Examination of our crystal structures revealed a new peptide-binding mode to the radixin FERM domain and provided several implications concerning the physiological role of NHERFs and ERM proteins. We identified determinant residues involved in NHERF peptide recognition by the radixin FERM domain and proposed the 13-residue Motif-2 distinct from Motif-1 for adhesion molecule recognition. Nonpolar interactions are dominant in the FERM-NHERF interaction, which is consistent with previous observations that FERM-NHERF binding is highly resistant to high-concentration (1-2 M) salt washes (Nguyen *et al.*, 2001). Key residues in direct interactions with the NHERF peptides are conserved in all members of ERM proteins (Fig. 3.8), indicating that NHERF binding to other members of ERM proteins would be essentially the same as those in our complexes. Moreover, most of these residues are also conserved in the merlin FERM domain, although non-homologous replacement of radixin Pro265 are found in loop β6C-β7C of merlin subdomain C. These merlin sequences may modify the pocket for the important tryptophan residue (Trp348 in NHERF-1) and would reduce the binding affinity to NHERFs (Reczek *et al.*, 1998). The key residues for NHERF binding are poorly conserved in the FERM domains of talin or the canonical PTB domains in other signaling proteins.

4.2 Data base search of the FERM binding motif-2

Using sequence database, we tried to find the NHERF-binding motif-2 in proteins that might interact with the FERM domain. The search with the consensus sequence, MDWxxxxx(L/I)Fxx(L/F), revealed NHERF and its homologues from various species from

SWISS-POLT and TrEMBL. The search using Wxxxxx(L/I)Fxx(L/F) resulted in finding of several proteins that have Motif-2 like sequence. These candidates are classified three types: multi-transmembrane proteins, adaptor proteins and nuclear proteins.

Multi-transmembrane proteins are three molecules. Longevity assurance homolog gene 1 (LAG1) is require for acyl-CoA dependent synthesis of ceramides containing very long acyl chain and is located in the endoplasmic reticulum (ER) (Venkataraman *et al.*, 2002). Probable phospholipid-transporting ATPase *DNF3* is one of the P-type ATPase encoded in the *Saccharomyces cerevisiae* gemone and seems to be flippase to concentrate Phosphatidylserine (PS) and phosphatidyletanolamine (PE) on the cytosolic side of the biological membranes (Hua *et al.*, 2002). Peroxisome assembly protein 12 (peroxin 12) is a RING-finger containing protein which plays a role in the translocation of peroxins (Chang *et al.*, 1997). These proteins localized in the organelles such as ER and peroxisome but not plasma membranes. For relationship between ERM proteins and the intracellular membrane system, Defacque H., *et al* reported that ERM proteins are involved in the actin assembly on phagosomal membranes (Defacque *et al.*, 2000). Also, proteomic analysis of the human B cell-derived exosome and melanoma-derived exosome reported that ERM proteins associated with these exosome (Wubbolts *et al.*, 2003: Hegmans *et al.*, 2004). These findings imply that ERM proteins may be related with regulation of the membrane proteins localized in the phagosome or exosome.

The second class of candidates contains adaptor proteins localized in the plasma or mitochondrial membranes. Ankyrin repeat and SOCS box protein 6 (ASB6) has six repeats of the ankyrin repeat and SOCS box (suppressor of cytokine signaling). ASB6 participated in the insulin receptor signaling through the association with the APS (Adaptor proteins with a pleckstrin homology and Src homology 2 domains) (Wilcox *et al.*, 2004). Signal

transducer and activator of transcription 1 (STAT1) is a latent cytoplasmic protein mediating cytokine signal and has a dual role as signal transducer and activator for transcription (Vinkemeier *et al.*, 2004). ASB6 and STAT1, localized at the plasma membrane, may be new binding partners targeted by ERM proteins, although FERM binding motif-2 of these proteins is middle of amino acid sequence. Bcl-2 binding component 3, also known as *PUMA* (p53 upregulated modulator of apoptosis), is the pro-apoptotic family member regulated by p53 tumour suppressor protein (Zhang *et al.*, 2001). This protein localized at mitochondria and plays a role for release of cytochrome *c* during p53 induced cell death (Schuler *et al.*, 2001). Although mitochondrial localization of the ERM proteins has been not reported, ERM proteins may be related with mitochondrial-dependent signal transductions, such as apoptosis.

Sentrin-specific protease 7 belongs to enzyme family which cleaved the isopeptide linkage between sentrin, also called SUMO-1 (small ubiquitin-related modifier), and various target proteins (Gong *et al.*, 2000). Down regulated in metastasis (DRIM) and suppressor of mar1-1 protein are DNA binding proteins that regulate gene expression in the nucleus (Chi *et al.*, 1996: Schwirzke *et al.*, 1998). Recently, Batchelor *et al* reported that ERM proteins localized in the nucleus (Batchelor *et al.*, 2004). These findings may imply that it is possible for ERM proteins to regulate gene expression through the interaction with these nucleus proteins containing motif 2.

4.3 Re-localization of the NHERF by cooperative binding effect.

As the number of known ERM target proteins that bind the FERM domain increases, so too will our understanding of the potential roles of competition between the targets or otherwise the cooperative binding of multiple targets. Target proteins that occupy

different binding sites on the FERM domain, and physiological signals that modify the FERM domain affinity for certain targets, thereby redirecting its function, needs to be explored. Using highly-purified protein and peptides, results of experiments presented here clearly revealed that the Motif-1 and the Motif-2 peptides compete for the radixin FERM domain. It is unlikely that the FERM domain can bridge two different membrane protein targets to coordinate their cellular function. The proposed competition between NHERF and adhesion molecules for ERM proteins is reminiscent of direct competition between β2AR and NHE3 for NHERF, which resolved a long standing paradox whereby some cAMP-elevating hormones inhibited NHE3 activity, while others like β2AR increased the activity (Hall, R.A. *et al.* 1998).

NHERFs are apical PDZ proteins highly expressed in epithelial cells. Molecular and cellular studies over the past decade have demonstrated that NHERFs regulate the apical targeting or trafficking of ion transporters and other membrane proteins (Shenolikar *et al.*, 2004). Consistent with the predominant localization of NHERFs at the apical cell surface, the growing list of potential NHERF targets shows a preponderance of membrane proteins such as ion transporters and receptors, specifically GPCRs. We suggest that competition between Motif-1 and Motif-2 peptides for binding to the FERM domain of ERM proteins facilitates switching between the apical and basolateral localization of membrane proteins. Recent studies have shown that NHERFs organizes ERM proteins at the apical membrane of polarized epithelia to maintain the brush border structures (Morales *et al.*, 2004). Moreover, NHERFs and its target, podocalyxin/gp135, participate in the formation of a preapical domain during polarization of MDCK cells (Meder *et al.*, 2005). These data indicate that functions of NHERF-ERM-F-actin scaffolding are expanding to include roles in cell polarization induction.

PDZ domain-mediated dimerization of NHERFs (Fouassier *et al.*, 2000, Shenolikar *et al.*, 2001, Lau *et al.*, 2001) has been shown to facilitate activation of receptors including PDGFR (Maudsley *et al.,* 2000) and CFTR (Raghuram *et al.*, 2001), while the dimerization exhibits rather low affinity compared with that for ERM-NHERF binding. NHERF-1 appeared to dimerize with K_d in the micromolar range (Shenolikar *et al.*, 2001). ERM proteins represent the most abundant cellular targets of NHERFs and the active open form of ERM proteins exist at or near the plasma membrane by anchoring to the actin cytoskeleton (Reczek *et al.*, 1997, Murthy *et al.*, 1998). Binding of NHERFs to the high-affinity binding target ERM proteins may determine the localization of NHERFs at the plasma membrane and effectively increase the local concentration of NHERFs, favoring dimerization and accelerating binding to membrane receptors and ion channels. This suggests that ERM proteins are important components of cellular complexes containing NHERF and play a role in regulating NHERF function.

4.4 Relationship with cancer

NHERF mRNA was recently identified as being highly induced by estrogen in estrogen-receptor (ER) positive breast cancer cells, and immuno-histochemical studies showed that NHERF expression was higher in breast tumors compared with the expression found in adjacent normal breast tissue (Voltz *et al.*, 2001). These data provide strong support suggesting that NHERF plays a role in tumor development. Given the proposed role of NHERF-1 in promoting PDGFR dimerization and activation of mitogenic signals, elevated NHERF-1 expression in breast cancer cells might accelerate cell proliferation. The NHERF-1 peptide or designed peptides that exhibit improved high-affinity binding to ERM proteins might antagonize NHERF-ERM binding, thereby

inhibiting cancer cell proliferation. Changes in Na^+/H^+ exchange play a role in tumor cell pseudopodial extensions (Lagana *et al.*, 2000). NHE3 may act in conjunction with NHERF to regulate the proliferation and invasive capacity of breast, ovarian and gastrointestinal cancers. Elevated NHERF expression, which stimulates cell proliferation, simultaneously weakens cell adhesion by sequestrating ERM proteins from adhesion molecules. This might provide one possible reason why the cancer cells easily detach from the tissue. NHERF peptides could prevent the metastatic nature of breast carcinoma.

4.5 Regulation of the FERM-NHERF interaction by phosphorylation

The NHERF C-terminal tail consisting of ca. 120 residues follows two PDZ domains. This long tail seems to be structurally flexible for the most part due to the presence of a serine-rich region spanning the N-terminal 90 residues of the tail. This region contains multiple phosphorylation sites, and is known to affect NHERF dimerization, thus facilitating activation of receptors including CFTR and PDGFR (Shenolikar *et al.*, 2004). The Ser-rich region containing the phosphorylation sites is located more than 50 residues from the FERM-binding region at the C-terminus. It seems unlikely that phosphorylation directly affects FERM binding, while the tail may fold back on itself, enabling the interaction between the phosphate group and the positively-charged region of the FERM binding region. Further work will be needed to define the effect of phosphorylation on FERM binding.

5, Acknowledgement

This work has been performed under the direction of Professor Toshio Hakoshima (Graduate School of Information Science, Nara Institute of Science and Technology). I would like to thank him for teaching me protein crystallography, for his guidance and support in the past five years. I would like to express deep gratitude to all members who belong(ed) to Hakoshima laboratory, especially to; Dr. Kengo Okada, Dr. Ryoko Maesaki for a lot of practical advices for protein crystallographic studies during all my work. I also wish to thank Dr. Ken Kitano, Dr. Hiroto Yamaguchi, Dr. Shigeru Sakurai for a lot of advices and support for my studies.

I would like to thank Dr. Sachiko Tsukita (Faculty of Medicine, Kyoto University, and College of medical Technology) for providing us the expression vectors of the radixin FERM domain.

I wish to thank Junko Tsukamoto for her technical support in performing MALDI-TOF-MS and N-terminal analysis.

Shin-ichi Terawaki

February 8, 2006

6, Reference

Abrahams, J.P. & Leslie A.G.W. Methods used in the structure determination of bovine mitochondrial F_1 ATPase. (1996) *Acta Crystallogr. D* **52**, 30-42.

Andréoli, C., Martin, M., Le Borgne, R., Reggio, H., and Mangeat, P. (1994) Ezrin has properties to self-associate at the plasma membrane. *J. Cell Sci.* **107**, 2509-2521

Alberts B, Johnson A, Lewis J, Raff M, Roberts K, Walter P. (2002) *Molecular Biology of the Cell* (third edition)

Alonso-Lebrero JL, Serrador JM, Dominguez-Jimenez C, Barreiro O, Luque A, del Pozo MA, Snapp K, Kansas G, Schwartz-Albiez R, Furthmayr H, Lozano F, Sanchez-Madrid F. (2000) Polarization and interaction of adhesion molecules P-selectin glycoprotein ligand 1 and intercellular adhesion molecule 3 with moesin and ezrin in myeloid cells. Blood. 95, 2413-9.

Barsukov IL, Prescot A, Bate N, Patel B, Floyd DN, Bhanji N, Bagshaw CR, Letinic K, Di Paolo G, De Camilli P, Roberts GC, Critchley DR. (2003) Phosphatidylinositol phosphate kinase type 1gamma and beta1-integrincytoplasmic domain bind to the same region in the talin FERM domain. *J Biol Chem.* **278**, 31202-31209.

Bonilha VL, Rodriguez-Boulan E. (2001) Polarity and developmental regulation of two PDZ proteins in the retinal pigment epithelium. *Invest Ophthalmol Vis Sci.* **42**, 3274-3282.

Bretscher A, Edwards K, Fehon RG. (2002) ERM proteins and merlin: integrators at the cell cortex. *Nat Rev Mol Cell Biol.* **3**, 586-599.

Bretscher A. (1983) Purification of an 80,000-dalton protein that is a component of the isolated microvillus cytoskeleton, and its localization in nonmuscle cells *J Cell Biol.* **97**, 425-432

Brünger, A.T. *et al.* (1998) Crystallography & NMR system: A new software suite for macromolecular structure determination. *Acta Crystallogr. D* **54**, 905-921.

Ceccarelli DF, Song HK, Poy F, Schaller MD, Eck MJ. (2005) Crystal structure of the FERM domain of focal adhesion kinase. *J Biol Chem. in press*

Chishti, A.H. *et al.* (1998) The FERM domain: a unique module involved in the linkage of cytoplasmic proteins to the membrane. *Trends Biochem. Sci.*, **23**, 281–282

Collaborative Computational Project, Number 4, The CCP4 suite: (1994) programs for protein crystallography. *Acta Crystallogr D* **50**, 760-763.

Dransfield DT, Bradford AJ, Smith J, Martin M, Roy C, Mangeat PH, Goldenring JR. (1997) Ezrin is a cyclic AMP-dependent protein kinase anchoring protein. *EMBO J.* **16**, 35-43.

Denker SP, Huang DC, Orlowski J, Furthmayr H, Barber DL. (2000) Direct binding of the Na--H exchanger NHE1 to ERM proteins regulates the cortical cytoskeleton and cell shape independently of H(+) translocation. *Mol Cell.* **6**, 1425-1436

de Pereda JM, Wegener KL, Santelli E, Bate N, Ginsberg MH, Critchley DR, Campbell ID, Liddington RC. (2005) Structural basis for phosphatidylinositol phosphate kinase type Igamma binding to talin at focal adhesions. *J Biol Chem.* **280**, 8381-8386.

Edwards SD, Keep NH. (2001) The 2.7 A crystal structure of the activated FERM domain of moesin: an analysis of structural changes on activation. *Biochemistry.* **40**, 7061-7068.

Fouassier L, Yun CC, Fitz JG, Doctor RB. (2000) Evidence for ezrin-radixin-moesin-binding phosphoprotein 50 (EBP50) self-association through PDZ-PDZ interactions. *J Biol Chem.* **275**, 25039-25045.

Fukata Y, Kimura K, Oshiro N, Saya H, Matsuura Y, Kaibuchi K. (1998) Association of the myosin-binding subunit of myosin phosphatase and moesin: dual regulation of moesin phosphorylation by Rho-associated kinase and myosin phosphatase. *J Cell Biol.*; **141,** 409-418.

Garcia-Alvarez B, de Pereda JM, Calderwood DA, Ulmer TS, Critchley D, Campbell ID, Ginsberg MH, Liddington RC. (2003) Structural determinants of integrin recognition by talin. *Mol Cell.* **11**, 49-58.

Gary, R., and Bretscher, A. (1995) Ezrin self-association involves binding of an N-terminal domain to a normally masked C-terminal domain that includes the F-actin binding site. *Mol. Biol. Cell.* **6,** 1061-1075

Gautreau A, Poullet P, Louvard D, Arpin M. (1999) Ezrin, a plasma membrane-microfilament linker, signals cell survival through the phosphatidylinositol 3-kinase/Akt pathway. *Proc Natl Acad Sci U S A.* **96**, 7300-7305.

Granes F, Urena JM, Rocamora N, Vilaro S. (2000) Ezrin links syndecan-2 to the cytoskeleton. *J Cell Sci.* **113**, 1267-1276

Hall, R.A. *et al.* (1998) The β_2-adrenergic receptor interacts with the Na^+/H^+-exchanger regulatory factor to control Na^+/H^+ exchange. *Nature.* **392**, 626–630.

Hamada K, Matsui T, Tsukita S, Tsukita S, Hakoshima T. (2000) Crystallographic characterization of the membrane-binding domain of radixin. *Acta Crystallogr. D* **56**, 922-923.

Hamada K, Shimizu T, Matsui T, Tsukita S, Hakoshima T. (2000) Structural basis of the membrane-targeting and unmasking mechanisms of the radixin FERM domain. *EMBO J.* **19**, 4449-4462.

Hamada K, Shimizu T, Yonemura S, Tsukita S, Tsukita S, Hakoshima T. (2003) Structural basis of adhesion-molecule recognition by ERM proteins revealed by the crystal structure of the radixin-ICAM-2 complex. *EMBO J.* **22**, 502-514.

Han BG, Nunomura W, Takakuwa Y, Mohandas N, Jap BK. (2000) Protein 4.1R core domain structure and insights into regulation of cytoskeletal organization. *Nat Struct Biol.* **7**, 871-875.

Hayashi K, Yonemura S, Matsui T, Tsukita S. (1999) Immunofluorescence detection of ezrin/radixin/moesin (ERM) proteins with their carboxyl-terminal threonine phosphorylated in cultured cells and tissues. *J Cell Sci.* **112**, 1149-1158.

Heiska L, Alfthan K, Gronholm M, Vilja P, Vaheri A, Carpen O. (1998) Association of ezrin with intercellular adhesion molecule-1 and -2 (ICAM-1 and ICAM-2). Regulation by phosphatidylinositol 4, 5-bisphosphate. *J Biol Chem.* **273**, 21893-21900.

Hirao M, Sato N, Kondo T, Yonemura S, Monden M, Sasaki T, Takai Y, Tsukita S, Tsukita S. (1996) Regulation mechanism of ERM (ezrin/radixin/moesin) protein/plasma membrane association: possible involvement of phosphatidylinositol turnover and Rho-dependent signaling pathway. J Cell Biol. **135**, 37-51.

Hu MC, Fan L, Crowder LA, Karim-Jimenez Z, Murer H, Moe OW. (2001) Dopamine acutely stimulates Na+/H+ exchanger (NHE3) endocytosis via clathrin-coated vesicles: dependence on protein kinase A-mediated NHE3 phosphorylation. J Biol Chem. **276**, 26906-26915.

Ivetic, A., Deka, J., Ridley, A. & Ager, A. (2001) The cytoplasmic tail of L-selectin interacts with members of the ezrin-radixin-moesin (ERM) family of proteins: activation dependent binding of moesin but not ezrin. *J. Biol. Chem.* **8**, 8.

Iwase A, Shen R, Navarro D, Nanus DM. (2004) Direct binding of neutral endopeptidase 24.11 to ezrin/radixin/moesin (ERM) proteins competes with the interaction of CD44 with ERM proteins. *J Biol Chem*. 279, 11898-11905.

Jones, T.A., Zou, J.-Y., Cowan, S.W. & Kjeldgaard, M. (1991) Improved methods for building protein models in electron density maps and the location of errors in these models. *Acta Crystallogr. A* **47**, 110-119.

Kotani H, Takaishi K, Sasaki T, Takai Y. (1997) Rho regulates association of both the ERM family and vinculin with the plasma membrane in MDCK cells. *Oncogene*. **14**, 1705-1713.

Khundmiri SJ, Weinman EJ, Steplock D, Cole J, Ahmad A, Baumann PD, Barati M, Rane MJ, Lederer E. (2005) Parathyroid hormone regulation of na+,k+-ATPase requires the PDZ 1 domain of sodium hydrogen exchanger regulatory factor-1 in opossum kidney cells. *J Am Soc Nephrol*. **16**, 2598-2607.

Kurashima K, D'Souza S, Szaszi K, Ramjeesingh R, Orlowski J, Grinstein S. (1999) The apical Na(+)/H(+) exchanger isoform NHE3 is regulated by the actin cytoskeleton. *J Biol Chem.* **274**, 29843-29849.

Kraulis, P.J. (1991). MOLSCRIPT - A program to produce both detailed and schematic plots of protein structures. J. Appl. Crystallogr. *24*, 946-950.

Kang BS, Cooper DR, Devedjiev Y, Derewenda U, Derewenda ZS. (2002) The structure of the FERM domain of merlin, the neurofibromatosis type 2 gene product. *Acta Crystallogr. D* **58**, 381-391.

Lagana, A. *et al.* (2000) Regulation of the formation of tumor cell pseudopodia by the Na^+/H^+ exchanger NHE1. *J. Cell Sci.* **113**, 3649-3662.

Lamb RF, Roy C, Diefenbach TJ, Vinters HV, Johnson MW, Jay DG, Hall A. (2000) The TSC1 tumour suppressor hamartin regulates cell adhesion through ERM proteins and the GTPase Rho. *Nat Cell Biol.* **2**, 281-287.

Lamprecht G, Weinman EJ, Yun CH. (1998) The role of NHERF and E3KARP in the cAMP-mediated inhibition of NHE3. *J Biol Chem.* **273**, 29972-29978.

Lankes W, Griesmacher A, Grunwald J, Schwartz-Albiez R, Keller R. (1988) A heparin-binding protein involved in inhibition of smooth-muscle cell proliferation. *Biochem J* . **251**, 831-842

Lankes WT, Furthmayr H. (1991) Moesin: a member of the protein 4.1-talin-ezrin family of proteins. *Proc Natl Acad Sci U S A.* **88**, 8297-8301

Lankes W, Griesmacher A, Grunwald J, Schwartz-Albiez R, Keller R. (1988) A heparin-binding protein involved in inhibition of smooth-muscle cell proliferation. *Biochem J.* **251**, 831-842.

Lau, A.G. & Hall, R.A. (2001) Oligomerization of NHERF-1 and NHERF-2 PDZ domains: differential regulation by association with receptor carboxyl-termini and by phosphorylation. *Biochemistry.* **40**, 8572–8580.

Lazar CS, Cresson CM, Lauffenburger DA, Gill GN. (2004) The Na+/H+ exchanger regulatory factor stabilizes epidermal growth factor receptors at the cell surface. *Mol Biol Cell.* 15, 5470-5480.

Lee JH, Katakai T, Hara T, Gonda H, Sugai M, Shimizu A. (2004) Roles of p-ERM and Rho-ROCK signaling in lymphocyte polarity and uropod formation. *J Cell Biol.* **167**, 327-337.

Legg JW, Isacke CM. (1998) Identification and functional analysis of the ezrin-binding site in the hyaluronan receptor, CD44. *Curr Biol.* **8**, 705-708.

Leslie, A.G.W. Joint CCP4 and EACMB Newsletter Protein Crystallography, Vol 26. Warrington, UK: Daresbury Laboratory (1992).

Magendantz, M., Henry, M. D., Lander, A., and Solomon, F. (1995) Interdomain Interactions of Radixin *in Vitro. J. Biol. Chem.* **270**, 25324-25327

Mahon, M.J., Donowitz, M., Yun, C.C. & Segre, G..V. (2002) Na^+/H^+ exchanger regulatory factor 2 directs parathyroid hormone 1 receptor signalling. *Nature.* **417**, 858-861.

Mahon MJ, Cole JA, Lederer ED, Segre GV. (2003) Na+/H+ exchanger-regulatory factor 1 mediates inhibition of phosphate transport by parathyroid hormone and second messengers by acting at multiple sites in opossum kidney cells. *Mol Endocrinol.* **17**, 2355-2364.

Manchanda N, Lyubimova A, Ho HY, James MF, Gusella JF, Ramesh N, Snapper SB, Ramesh V. (2005) The NF2 tumor suppressor Merlin and the ERM proteins interact with N-WASP and regulate its actin polymerization function. *J Biol Chem.* **280**, 12517-12522.

Matthews, B. W. (1968). *J. Mol. Biol.* **33**, 491-497.

Matsui T, Maeda M, Doi Y, Yonemura S, Amano M, Kaibuchi K, Tsukita S, Tsukita S. (1998) Rho-kinase phosphorylates COOH-terminal threonines of ezrin/radixin/moesin (ERM) proteins and regulates their head-to-tail association. *J Cell Biol.* **140**, 647-657.

Matsui T, Yonemura S, Tsukita S, Tsukita S. (1999) Activation of ERM proteins in vivo by Rho involves phosphatidyl-inositol 4-phosphate 5-kinase and not ROCK kinases. *Curr Biol.*; **9**, 1259-1262.

Maudsley, S. *et al.* (2000) Platelet-derived growth factor receptor association with Na^+/H^+ exchanger regulatory factor potentiates receptor activity. *Mol. Cell. Biol.* **20**, 8352–8363.

Meder, D., Shevchenko, A., Simons, K. & Füllekrug, J. (2005) Gp135/podocalyxin and NHERF-2 participate in the formation of a preapical domain during polarization of MDCK cells. *J. Cell Biol.* **168**, 303-313.

Morales, F.C., Takahashi , Y., Kreimann, E.L. & Georgescu, M.-M. (2004) Ezrin–radixin–moesin (ERM)-binding phosphoprotein 50 organizes ERM proteins at the apical membrane of polarized epithelia. *Proc. Natl. Acad. Sci. USA* **101**, 17705-17710.

Murshudov, G.N., Vagin, A.A. & Dodson, E.J. (1997) Refinement of macromolecular structures by the maximum-likelihood method. *Acta Crystallogr. D* **53**, 240-255.

Murthy, A. *et al.* (1998) NHE-RF, a regulatory cofactor for Na^+-H^+ exchange, is a common interactor for merlin and ERM (MERM) proteins. *J. Biol. Chem.* **273**, 1273-1276.

Navaza, J. (1994) AMoRe: An automated package for molecular replacement. *Acta Crystallogr. A* **50**, 157-163.

Nguyen, R., Reczek, D. & Bretscher, A. (2001) Hierarchy of merlin and ezrin N- and C-terminal domain interactions in homo-and heterotypic associations and their relationship to binding of scaffolding proteins EBP50 and E3KARP. *J. Biol. Chem.* **276**, 7621–7629.

Ng T, Parsons M, Hughes WE, Monypenny J, Zicha D, Gautreau A, Arpin M, Gschmeissner S, Verveer PJ, Bastiaens PI, Parker PJ. (2001) Ezrin is a downstream effector of trafficking PKC-integrin complexes involved in the control of cell motility. *EMBO J.* **20**, 2723-2741.

Oshiro N, Fukata Y, Kaibuchi K. (1998) Phosphorylation of moesin by rho-associated kinase (Rho-kinase) plays a crucial role in the formation of microvilli-like structures. *J Biol Chem.* **273**, 34663-34666.

Otwinowski, Z. & Minor, W. (1997) Processing of X-ray diffraction data collected in oscillation mode. *Methods Enzymol.* **276**, 307-326.

Parlato S, Giammarioli AM, Logozzi M, Lozupone F, Matarrese P, Luciani F, Falchi M, Malorni W, Fais S. (2000) CD95 (APO-1/Fas) linkage to the actin cytoskeleton through ezrin in human T lymphocytes: a novel regulatory mechanism of the CD95 apoptotic pathway. *EMBO J.* **19**, 5123-5134.

Pearson MA, Reczek D, Bretscher A, Karplus PA. (2000) Structure of the ERM protein moesin reveals the FERM domain fold masked by an extended actin binding tail domain. *Cell.* **101**, 259-270

Pietromonaco SF, Simons PC, Altman A, Elias L. (1998) Protein kinase C-theta phosphorylation of moesin in the actin-binding sequence. *J Biol Chem.* **273**, 7594-7603.

Poullet P, Gautreau A, Kadare G, Girault JA, Louvard D, Arpin M. (2001) Ezrin interacts with focal adhesion kinase and induces its activation independently of cell-matrix adhesion. *J Biol Chem*. **276**, 37686-37691.

Reczek D, Berryman M, Bretscher A. (1997) Identification of EBP50: A PDZ-containing phosphoprotein that associates with members of the ezrin-radixin-moesin family. *J Cell Biol*. **139**, 169-179.

Reczek, D. & Bretscher, A. (1998) The carboxyl-terminal region of EBP50 binds to a site in the amino-terminal domain of ezrin that is masked in the dormant molecule. *J. Biol. Chem.* **273**, 18452-18458.

Raghuram V, Mak DD, Foskett JK. (2001) Regulation of cystic fibrosis transmembrane conductance regulator single-channel gating by bivalent PDZ-domain-mediated interaction. *Proc Natl Acad Sci U S A*. **98**, 1300-1305.

Sato N, Funayama N, Nagafuchi A, Yonemura S, Tsukita S, Tsukita S. (1992) A gene family consisting of ezrin, radixin and moesin. Its specific localization at actin filament/plasma membrane association sites. *J Cell Sci*. **103**, 131-143

Shaw RJ, Henry M, Solomon F, Jacks T. (1998) RhoA-dependent phosphorylation and relocalization of ERM proteins into apical membrane/actin protrusions in fibroblasts. *Mol Biol Cell*. **9**, 403-419.

Simons PC, Pietromonaco SF, Reczek D, Bretscher A, Elias L. (1998) C-terminal threonine phosphorylation activates ERM proteins to link the cell's cortical lipid bilayer to the cytoskeleton. *Biochem Biophys Res Commun*. **253**, 561-565.

Sun F, Hug MJ, Lewarchik CM, Yun CH, Bradbury NA, Frizzell RA. (2000) E3KARP mediates the association of ezrin and protein kinase A with the cystic fibrosis transmembrane conductance regulator in airway cells. *J Biol Chem*. **275**, 29539-29546.

Shenolikar S, Minkoff CM, Steplock DA, Evangelista C, Liu M, Weinman EJ. (2001) N-terminal PDZ domain is required for NHERF dimerization. *FEBS Lett*. **489**, 233-236.

Shenolikar, S., Voltz, J.W., Cunningham, R. & Weinman, E.J. (2004) Regulation of ion transport by the NHERF family of PDZ proteins. *Physiology* **19**, 362-369.

Smith WJ, Nassar N, Bretscher A, Cerione RA, Karplus PA. (2003) Structure of the active N-terminal domain of Ezrin. Conformational and mobility changes identify keystone interactions. *J Biol Chem*. **278**, 4949-4956.

Shimizu T, Seto A, Maita N, Hamada K, Tsukita S, Tsukita S, Hakoshima T. (2002) Structural basis for neurofibromatosis type 2. Crystal structure of the merlin FERM domain. *J Biol Chem*. **277**, 10332-10336.

Takahashi K, Sasaki T, Mammoto A, Takaishi K, Kameyama T, Tsukita S, Takai Y. (1997) Direct interaction of the Rho GDP dissociation inhibitor with ezrin/radixin/moesin initiates the activation of the Rho small G protein. *J Biol Chem*. **272**, 23371-23375.

Takahashi K, Sasaki T, Mammoto A, Hotta I, Takaishi K, Imamura H, Nakano K, Kodama A, Takai Y. (1998) Interaction of radixin with Rho small G protein GDP/GTP exchange protein Dbl. *Oncogene*. **16**, 3279-3284.

Terawaki S, Maesaki R, Okada K, Hakoshima T. (2003) Crystallographic characterization of the radixin FERM domain bound to the C-terminal region of the human Na+/H+-exchanger regulatory factor (NHERF). *Acta Crystallogr. D* **59**, 177-179.

Tran Quang C, Gautreau A, Arpin M, Treisman R. (2000) Ezrin function is required for ROCK-mediated fibroblast transformation by the Net and Dbl oncogenes. *EMBO J.* **19**, 4565-4576.

Tsukita S, Hieda Y, Tsukita S. (1989) A new 82-kD barbed end-capping protein (radixin) localized in the cell-to-cell adherens junction: purification and characterization. *J Cell Biol.* **108**, 2369-2382

Tsukita S, Oishi K, Sato N, Sagara J, Kawai A, Tsukita S. (1994) ERM family members as molecular linkers between the cell surface glycoprotein CD44 and actin-based cytoskeletons. *J Cell Biol*. **126**, 391-401.

Tsukita,S. and Yonemura,S. (1999) Cortical actin organization: lessons from ERM (ezrin/radixin/moesin) proteins. *J. Biol. Chem.* **274**, 34507–34510

Tsukita S, Oishi K, Sato N, Sagara J, Kawai A, Tsukita S. (1994)ERM family members as molecular linkers between the cell surface glycoprotein CD44 and actin-based cytoskeletons. *J Cell Biol.* **126**, 391-401

Turunen, O., Wahlstrom, T. & Vaheri, A. (1994) Ezrin has a COOH-terminal actin-binding site that is conserved in the ezrin protein family. *J. Cell Biol.* **126**, 1445-1453.

Vanni C, Parodi A, Mancini P, Visco V, Ottaviano C, Torrisi MR, Eva A. (2004) Phosphorylation-independent membrane relocalization of ezrin following association with Dbl in vivo. *Oncogene*. **23**, 4098-4106.

Voltz JW, Weinman EJ, Shenolikar S. (2001) Expanding the role of NHERF, a PDZ-domain containing protein adapter, to growth regulation. *Oncogene*. **20**, 6309-6314.

Wang, S., Raab, R.W., Schatz, P.J., Guggino, W.B. & Li, M. (1998) Peptide binding consensus of the NHE-RF-PDZ1 domain matches the C-terminal sequence of cystic fibrosis transmembrane conductance regulator (CFTR). *FEBS Lett.* **427**, 103–108.

Weinman EJ, Steplock D, Shenolikar S. (1993) CAMP-mediated inhibition of the renal brush border membrane Na+-H+ exchanger requires a dissociable phosphoprotein cofactor. *J Clin Invest*. **92**, 1781-1786.

Weinman EJ, Steplock D, Donowitz M, Shenolikar S. (2000) NHERF associations with sodium-hydrogen exchanger isoform 3 (NHE3) and ezrin are essential for cAMP-mediated phosphorylation and inhibition of NHE3. *Biochemistry*. **39**, 6123-6129.

Weinman, E.J., Steplock, D., Wang, Y. & Shenolikar, S. (1995) Characterization of a protein cofactor that mediates protein kinase A regulation of the renal brush border membrane Na^+-H^+ exchanger. *J Clin. Invest.* **95**, 2143-2149.

Weinman EJ, Minkoff C, Shenolikar S. (2000) Signal complex regulation of renal transport proteins: NHERF and regulation of NHE3 by PKA. *Am J Physiol Renal Physiol*. **279**, 393-399.

Yonemura S, Hirao M, Doi Y, Takahashi N, Kondo T, Tsukita S, Tsukita S. (1998) Ezrin/radixin/moesin (ERM) proteins bind to a positively charged amino acid cluster in the juxta-membrane cytoplasmic domain of CD44, CD43, and ICAM-2. *J Cell Biol*. **140**, 885-895.

Yonemura S, Matsui T, Tsukita S, Tsukita S. (2002) Rho-dependent and -independent activation mechanisms of ezrin/radixin/moesin proteins: an essential role for polyphosphoinositides in vivo. *J Cell Sci*. **115**, 2569-2580.

Yun CH, Lamprecht G, Forster DV, Sidor A. (1998) NHE3 kinase A regulatory protein E3KARP binds the epithelial brush border Na+/H+ exchanger NHE3 and the cytoskeletal protein ezrin. *J Biol Chem*. **273**, 25856-25863.